ELSEVIER

Palaeogeography, Palaeoclimatology, Palaeoecology 141 (1998) 303–328

PALAEO

Palaeoenvironmental implications and diagenesis of inoceramid shells (Bivalvia) in the mid-Maastrichtian beds of the Sopelana, Zumaya and Bidart sections (coast of the Bay of Biscay, Basque Country)

J. Elorza *, F. García-Garmilla

Departamento Mineralogía y Petrología, Universidad del País Vasco, Apdo. 644, 48080-Bilbao, Bizkaia, Spain

Received 10 June 1996; accepted 2 February 1998

Abstract

Inoceramid bivalve shells from the mid-Maastrichtian beds of the Sopelana, Zumaya and Bidart sections in the Basque Country, were tested for their post-depositional diagenetic alteration. Petrography, cathodoluminescence (CL) and scanning electron microscope (SEM) observations together with geochemical analyses, indicate that the coarsely prismatic calcite of the shells from the Sopelana and Zumaya sections have undergone diagenetic alteration, without there being substantial textural changes in the original prismatic microstructure. A generalized bright yellowish to red colour is seen in all the samples observed by CL. The $\delta^{18}O$ values obtained from the shell prisms range from $-2.94‰$ to $-5.18‰$, with a mean value of $-3.6 \pm 0.5‰$ in the Sopelana section, whereas in the Zumaya section they range from $-1.88‰$ to $-4.71‰$, with a mean value of $-3.2 \pm 0.3‰$. These values are clearly lower than those from the Bidart section (from $-0.32‰$ to $-1.48‰$; mean value $-0.7 \pm 0.3‰$). Other evidence of diagenetic alteration is inferred from both whole-shell geochemistry and microprobe analysis. A complementary zonation in the distribution of 'diagenetic tracers' can be detected from the inner shell layer (ISL) to the outer shell layer (OSL) of inoceramid shells, together with a rare earth element (REE) enrichment in the shells which have lighter $\delta^{18}O$ values. In contrast, the inoceramid bivalve shells and their host-rock from the Bidart section were less altered. The calculated mean palaeotemperature (15ºC) and the value of 13ºC estimated from the non-luminescent middle shell layer seem to be consistent with palaeolatitudes about 30ºN for deep marine waters of mid-Maastrichtian time, as the last step of the long-term climatic cooling of the Late Cretaceous 'greenhouse'.

Keywords: inoceramid bivalves; isotopes; cathodoluminescence; palaeotemperatures; diagenesis; mid-Maastrichtian; Basque Arc domain

1. Introduction

Since the 1980's many papers on comparative geochemical studies (analyses of stable isotopes, minor and trace elements) of recent mollusk shells and fossil shells have appeared in the literature. The aim of the research by Morrison and Brand (1984, 1986, 1988); Brand (1986, 1987); Veizer et al. (1986); Krantz et al. (1987); Brand and Morrison (1987); Barrera and Tevesz (1990) and Barrera et al. (1990), among others, was mainly to characterize the

* Corresponding author. Fax: 34 4 464 8500; E-mail: nppelzaj@lg.ehu.es

0031-0182/98/$19.00
PII S0031-0182(98)00058-3

palaeoenvironmental features at different latitudes and sedimentary settings. Other objectives included: the construction of behaviour models of oceanic water columns based on the isotopic record (C, O, Sr, Nd), the REE content and the elemental geochemistry of Cretaceous inoceramid and ammonite shells from sediments from the Interior Seaway (Whittaker et al., 1987; Whittaker and Kyser, 1993) and Antarctica (Pirrie and Marshall, 1990a). It is generally assumed that the final composition of fossil shells is determined by: (a) the physical/chemical environment in which the organism lived; (b) the biological controls during skeletal growth; and (c) the subsequent diagenetic alteration undergone by the shell (Dodd and Stanton, 1981).

Deep Sea Drilling Project (DSDP) results reveal that inoceramid bivalves lived in all of the world's oceans at different depths (from shelfal to abyssal palaeodepths), from tropical to austral palaeolatitudes in Late Cretaceous sediments (Saito and Van Donk, 1974; Saltzman and Barron, 1982; Barron et al., 1984; MacLeod et al., 1996) and their frequency shows fluctuations partly in response to changes in sea level. Regressions and lowstands correspond to a rise in the total number of species (Voigt, 1995). Saltzman and Barron (1982) and Barron et al. (1984) selected inoceramid shells apparently unaffected by diagenesis and did not take into account the possible 'vital effect'. Oxygen isotopic analyses indicated that deep-water palaeotemperatures were significantly decreased during the Coniacian, Campanian and particularly during the Maastrichtian throughout the South Atlantic, Pacific and Indian Oceans.

Inoceramids have also been studied from a biostratigraphic point of view and also with regard to their extinction pattern during the mid-Maastrichtian in the Basque Arc domain (Ward et al., 1986; Ward, 1988; Wiedmann, 1988a,b; Ward et al., 1991; MacLeod and Orr, 1993; MacLeod, 1994) and in the Navarro–Cantabrian Trough (López, 1992; López et al., 1992), both domains belonging to the Basque–Cantabrian Basin, as defined by Feuillée and Rat (1971). The decline of inoceramids in the K/T stratigraphic record has also served to show gradual changes in ecological conditions (MacLeod and Orr, 1993; MacLeod, 1994).

Furthermore, it is worth noting that several aspects of the diagenesis undergone by inoceramid shells have been less studied, i.e. the attack paths through which the alteration progressed, the role of growth bands as geochemical controls of alteration, the zones of the shell most susceptible to diagenetic modification, and finally the geochemical variations in the isotopic record, and in the content of minor and trace elements and REE's in the shells. These and other aspects have been investigated, in lower Santonian inoceramid shells of the Basque Arc domain (Elorza and García-Garmilla, 1996), which were clearly affected by burial diagenesis. In the present paper, we describe a comparative study of inoceramid shells collected from the coastal exposures in Sopelana, Zumaya and Bidart (Fig. 1). Although inoceramid shells from each section experienced very similar environmental conditions and have the same geological age (mid-Maastrichtian), the CL and SEM observations, C and O isotope data, inoceramid shell/whole-rock geochemical ratios and electronic microprobe results lead us to think that the diagenetic history was relatively similar in the sections of Sopelana and Zumaya, but essentially different in the Bidart section.

2. Geological setting

Hemipelagic carbonate-rich, Maastrichtian sediments of the Basque Arc domain are very well exposed along the coast of the Bay of Biscay. For this reason and because several sections preserve the K/T boundary, these sediments have been the focus of considerable research. Rat (1959) contributed to a better knowledge of the regional geology of the Basque–Cantabrian Basin and pointed out some complete sections of Maastrichtian sediments. Later studies have described stratigraphy, sedimentology and palaeogeography (Mathey, 1982, 1987, 1988), biostratigraphy using foraminifera (von Hillebrandt, 1965; Lamolda et al., 1983), ammonoids and/or inoceramids (Ward et al., 1986; Wiedmann, 1988a,b; Ward, 1988; Ward et al., 1991; Ward and Kennedy, 1993), and nannoplankton (Percival and Fischer, 1977; Burnett et al., 1992; Gorostidi, 1993). Stable isotope studies (Mount et al., 1986; Margolis et al., 1987; Clauser, 1987, 1994; Nelson et al., 1991; McArthur et al., 1992; Ward et al., 1992), magnetostratigraphy (Delacotte, 1982; Delacotte et al.,

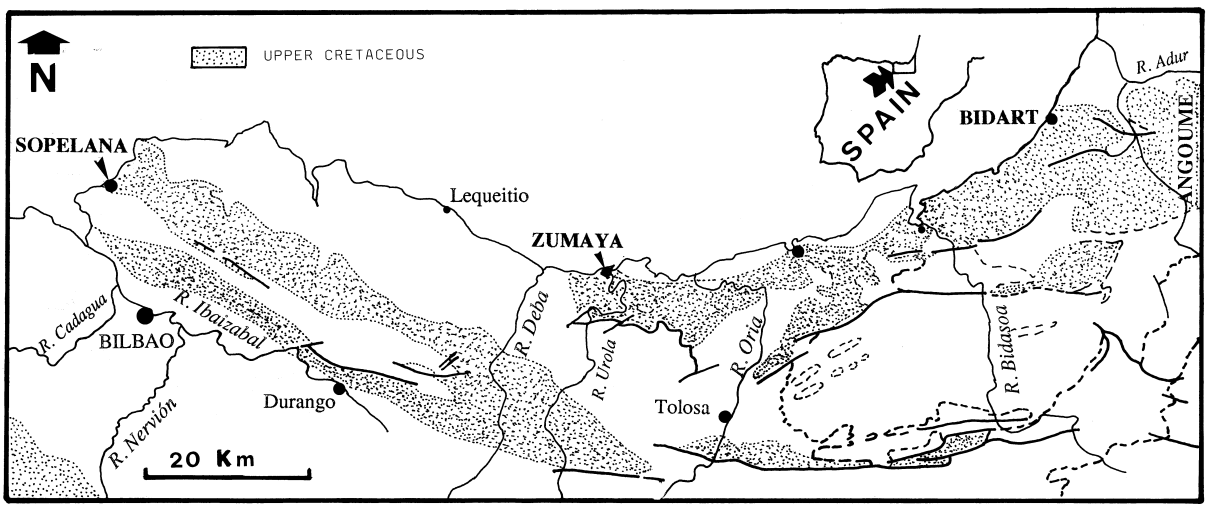

Fig. 1. Geographic and geological location of the Sopelana, Zumaya and Bidart sections, belonging to the lower–mid-Maastrichtian (Bay of Biscay).

1985; Mary et al., 1991), and studies about marly limestone/marl cyclicity, as a response to variations in siliciclastic inputs (Mount and Ward, 1986) have been published.

Our work focuses on three well-known sections: Sopelana, Zumaya, and Bidart, which contain seemingly well-preserved inoceramid shells. The three sections exhibit an alternation of layered marl and marly-limestone, typically 20–30 cm thick (Figs. 2 and 3A, B), as well as occasional, thin distal turbiditic sandstones (specifically in the Zumaya section). The sediments were deposited in a pelagic/hemipelagic environment which persisted during the Maastrichtian (Mathey, 1982, 1987). Five lithostratigraphic members were recognized by MacLeod and Ward (1990), which maintain the same lithologic alternations although with different thicknesses in each section. Inoceramids are most abundant in the so-called Member I, belonging to the *Gansserina gansseri* biozone and do not reach the *Abathomphalus mayaroensis* biozone. They eventually disappear in the upper part of Member II, coinciding with the nannofossil zone 24 to 25A, which is contemporaneous with the *Anapachydiscus fresvillensis* ammonite zone, in magnetochron 31N (summarized by MacLeod and Orr, 1993). Six different species of inoceramids have been identified (MacLeod and Ward, 1990; Ward et al., 1991; MacLeod, 1994). Most inoceramid shells, sometimes colonized by small oyster shells, appear complete both in marly and marly-limestone sediments, but they are particularly abundant at the top of the marly-limestone horizons (Fig. 3C, D).

3. Analytical methods

A selection of 50 thin sections of inoceramid samples were prepared for standard transmitted light petrography, CL and carbonate staining with Alizarin Red S and potassium ferricyanide (following Dickson, 1965). Fragments of inoceramid prismatic calcite shell material were selected and examined under SEM using a Jeol JSM-T6400 at the Universidad del País Vasco.

All CL work employed a Technosyn Cold Cathode Luminescence system, model 8200 Mk II, mounted on an Olympus triocular research microscope with a maximum magnification capability of 400×, utilizing universal stage objectives. Standard operating conditions included an accelerating potential of 12 kV and a 0.5–0.6 mA beam current with a beam diameter of approximately 5 mm.

The stable isotope values of $^{18}O/^{16}O$ and $^{13}C/^{12}C$ from inoceramid shells and bulk-rock (marly-limestones and marls), selected from the three sections, were determined by using a VG SIRA-9 mass spectrometer at the Universidad de Barcelona and Uni-

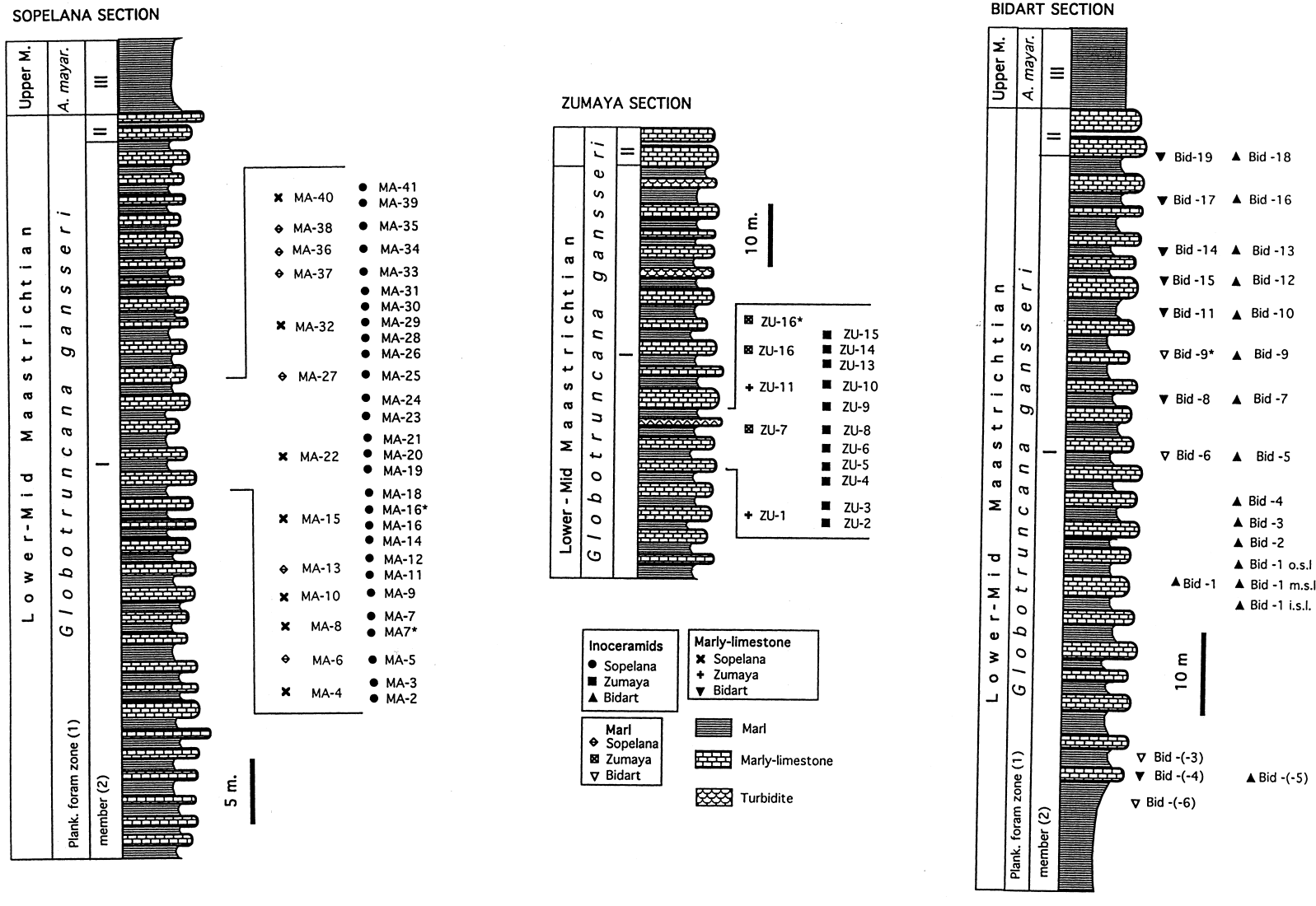

Fig. 2. Simplified and partial stratigraphic columns of the Sopelana, Zumaya and Bidart cliffs showing the different lithostratigraphic members (*I–III*), the planktonic foraminiferal biozone (*Globotruncana gansseri* and *Abathomphalus mayaroensis*) and the location of inoceramid samples collected together with the host-rock (marl or marly-limestone) which are described in the text. References: (*1*) MacLeod and Orr (1993); (*2*) MacLeod and Ward (1990).

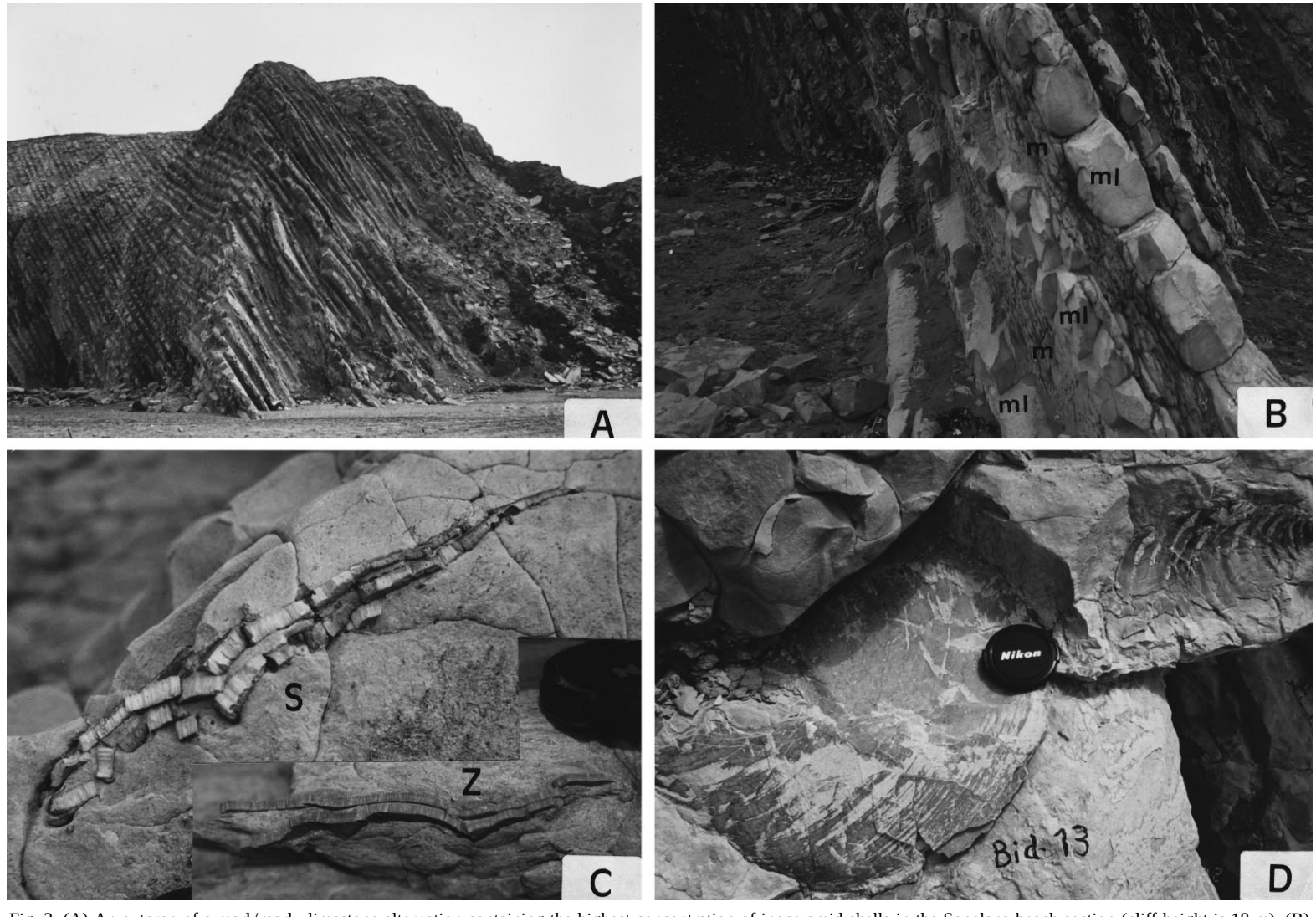

Fig. 3. (A) An outcrop of a marl/marly-limestone alternation containing the highest concentration of inoceramid shells in the Sopelana beach section (cliff height is 18 m). (B) A detail of the previous photograph (*m* = marl, *ml* = marly-limestone). (C) Two different sections of inoceramid shells contained in marly-limestones. Both specimens exhibit two complete but fractured valves, and the prismatic structure can be easily observed. S is a specimen from Sopelana and Z is from Zumaya. The lens cap is 5 cm in diameter. (D) Two almost complete inoceramid shells (sample BID-13) from Bidart. The lens cap is 5 cm in diameter.

versidad de Salamanca (Spain). Extraction of CO_2 from carbonates was carried out according to the method described by McCrea (1950). The results are expressed in δ notation in ‰, relative to the Pee Dee Belemnite (PDB) standard: calcite palaeotemperature values (in ºC) were calculated by using the equation of Craig (1965):

$$t = 16.9 - 4.2(\delta_c - \delta_w) + 0.13(\delta_c - \delta_w)^2$$

where δ_c is $\delta^{18}O$ of CO_2 generated by reaction of the carbonate with H_3PO_4 at 25ºC (PDB), and δ_w is $\delta^{18}O$ of the water relative to standard mean ocean water (SMOW). Reproducibility for both $\delta^{18}O$ and $\delta^{13}C$ is better than 0.1‰. A value of −1.0‰ (SMOW) was taken for non-glacial Cretaceous sea water as assumed by Lowenstam (1964) and Carson (1987), equivalent to −1.2‰ PDB for the above equation (see Pirrie and Marshall, 1990a).

The inoceramid shells and associated host rock from each of the three sections which had the lowest and highest $\delta^{18}O$ values, were examined for their content of major, minor and trace elements (21 elements in total) and of REEs (14 elements). Inoceramid shells and bulk-rock samples were powdered in a tungsten-carbide mill. Major elements (wt%) and Sc (ppm) were determined by inductively coupled plasma (ICP) emission spectrometry. Samples for trace element and REE analyses were fused with ultrapure lithium metaborate flux, dissolved while molten in HNO_3, and analyzed on a VG PlasmaQuad PQ22, inductively coupled plasma source mass spectrometer (ICP–MS) at the Centre de Recherches Pétrographiques et Géochimiques (Nancy, France), following techniques described by Govindaraju and Mevelle (1987). The detection limits are incorporated in Table 2.

In addition, thin sections of inoceramid shells from each of the Sopelana, Zumaya, and Bidart sections were polished, to determine the Fe, Mn, Na, Sr, and Mg contents, using an automatic Camebax microprobe at the Département des Sciences de la Terre of the Université Blaise Pascal in Clermont-Ferrand (France). Operating conditions were: 10 s counting time, ca. 10 nA beam current and the primary beam spot was focused to a diameter of ca. 2 μm with 15 kV accelerating voltage. Calibration was against Bureau de Recherches Géologiques et Miniérès (French Geological Survey) standard minerals, and a ZAF (correction program) was used (Henoc and Tong, 1978). The chemical composition of inoceramid shells was recalculated as mole percent of $CaCO_3$, $MgCO_3$ and $(Fe + Mn)CO_3$ (Table 3).

4. Results

4.1. Petrography of inoceramid shells

We examined 50 thin sections of inoceramids (cut from both complete shells and large shell fragments (>200 mm), with thick and thin walls, and some small adjoined specimens of oysters, found in the marly and marly-limestone sediments of the Sopelana, Zumaya and Bidart coastal exposures. Inoceramid shell thickness ranged from 1 to 4 mm (see Table 1). Under the microscope, the regular, simple prismatic calcitic microstructure of the inoceramid shells and the composite foliated and vesicular microstructure of the oysters were apparent. Each inoceramid prism corresponds to a single crystal and is about 0.1 mm wide and from 1 mm to 3 mm in length. Usually, prism diameters and their polygonal shapes appear rather uniform in sections cut perpendicular to the prisms' long axis, but prism diameters decrease notably from the inner shell layer (ISL) towards the outer part of the layer (OSL). Growth lines occur and are visible perpendicular to the prisms' long axes. The coarsest lines (0.2–0.5 mm spacing) are well preserved, whereas the finest ones (0.01–0.02 mm spacing) are sometimes difficult to distinguish (Fig. 4A, C, E).

We have not observed the inner aragonitic nacreous shell layer described by other authors in different areas (Wright, 1987; Whittaker et al., 1987; Pirrie and Marshall, 1990a). The boundary between prisms is clearly defined and well marked, and in some cases is penetrated by replacive silica. The latter consists of quartzine–lutecite spherules together with small bands of the same composition covering the edges of the shell fragments, in a way similar to that observed by Elorza and García-Garmilla (1996) in the Barrika section (lower Santonian) of the same Basque Arc domain.

In these thin sections, the inoceramid prisms of the shells collected from the Sopelana and Zumaya sections show under CL a generalized bright yel-

Table 1
Summary of isotopic data, thickness and estimated paleotemperatures for inoceramid shells, together with marl and marly-limestone samples from the Sopelana, Zumaya and Bidart sections

Sample	Mineralogy	Lithology host-rock	Thickness shell (mm)	δ^{18}O‰ (PDB)	δ^{13}C‰(PDB)	t (ºC)
SOPELANA SECTION						
Inoceramid						
MA-41	Calcite	Marly-limest.	>2	−4.46	2.2	28.8
MA-39	Calcite	Marly-limest.	>2	−4.24	2.42	28.0
MA-35	Calcite	Marl	>3	−3.98	1.98	27.2
MA-34	Calcite	Marl	>2	−3.42	1.67	25.3
MA-33	Calcite	Marl	>4	−5.18	1.46	31.0
MA-31	Calcite	Marly-limest.	>2	−3.57	2.29	25.8
MA-30	Calcite	Marly-limest.	>2	−4.05	1.83	27.4
MA-29	Calcite	Marly-limest.	>2.5	−3.52	2.17	25.6
MA-28	Calcite	Marly-limest.	>2.5	−3.54	2.1	25.7
MA-26	Calcite	Marly-limest.	>2	−3.98	2.05	27.2
MA-25	Calcite	Marl	>1	−3.25	1.74	24.7
MA-24	Calcite	Marly-limest.	>2	−3.53	1.88	25.6
MA-23	Calcite	Marly-limest.	>1.5	−3.57	1.63	25.8
MA-21	Calcite	Marly-limest.	>2	−3.97	1.32	27.1
MA-20	Calcite	Marly-limest.	>3	−3.52	2.18	25.6
MA-19	Calcite	Marly-limest.	>1.5	−3.38	1.9	25.1
MA-18	Calcite	Marly-limest.	>1	−3.45	2.06	25.4
MA-16′	Calcite	Marly-limest.	>1	−3.21	1.87	24.5
MA-16	Calcite	Marly-limest.	>1	−3.55	1.86	25.7
MA-14	Calcite	Marly-limest.	>2	−3.14	1.75	24.3
MA-12	Calcite	Marl	>3	−3.08	1.78	24.0
MA-11	Calcite	Marl	>1.5	−3.41.	1.39	25.2
MA-9	Calcite	Marly-limest.	>2	−3.56	2.53	25.7
MA-7′	Calcite	Marly-limest.	>1.5	−3.14	1.89	24.3
MA-7	Calcite	Marly-limest.	>1.5	−3.62	1.89	25.9
MA-5	Calcite	Marl	>1	−3.13	2.08	24.2
MA-3	Calcite	Marly-limest.	>3	−3.14	1.69	24.3
MA-2	Calcite	Marly-limest.	>1	−2.94	2.03	23.5
Mean value of inoceramids ($n = 28$)				−3.6±0.5	1.9±0.3	25.8
Marls associated with inoceramids						
MA-6		Marls		−3.95	1.88	
MA-13		Marls		−3.98	1.83	
MA-27		Marls		−4.20	1.77	
MA-37		Marls		−4.23	1.73	
MA-36		Marls		−3.98	1.80	
MA-38		Marls		−4.27	1.77	
Mean value of marls ($n = 6$)				−4.1±0.1	1.8±0.05	
Marly-limestones associated with inoceramids						
Ma-4		Marly-limest.		−4.51	1.88	
MA-8		Marly-limest.		−4.30	1.83	
MA-10		Marly-limest.		−3.98	1.77	
MA-10′		Marly-limest.		−3.96	1.86	
MA-15		Marly-limest.		−3.96	1.86	
MA-22		Marly-limest.		−4.10	1.86	
MA-32		Marly-limest.		−4.09	1.92	
MA-40		Marly-limest.		−4.37	1.77	
Mean value of marly-limestones ($n = 8$)				−4.1±0.2	1.8±0.05	
ZUMAYA SECTION						
Inoceramids						
ZU-15	Calcite	Marl	>2	−4.71	2.32	30.0
ZU-14	Calcite	Marl	>2	−4.01	2.28	27.7

Table 1 (continued)

Sample	Mineralogy	Lithology host-rock	Thickness shell (mm)	δ^{18}O‰ (PDB)	δ^{13}C‰(PDB)	t (ºC)
ZU-13	Calcite	Marl	>1	−1.88	2.17	19.7
ZU-10	Calcite	Marly-limest.	>2	−3.26	2.38	25.0
ZU-9	Calcite	Marly-limest.	>2	−2.81	2.26	23.3
ZU-8	Calcite	Marl	>1	−3.38	1.58	25.4
ZU-6	Calcite	Marl	>1.5	−2.79	2.48	23.2
ZU-5	Calcite	Marl	>2	−3.26	1.92	25.0
ZU-4	Calcite	Marl	>1.5	−3.12	2.25	24.5
ZU-3	Calcite	Marly-limest.	>3	−3.01	2.59	24.1
ZU-2	Calcite	Marly-limest.	>1	−2.59	2.30	22.5
Mean value of inoceramids ($n = 11$)				−3.2±0.7	2.2±0.3	24.6
Marls associated with inoceramids						
ZU′-16		Marls		−3.13	1.66	
ZU-16		Marls		−3.30	1.58	
ZU-7		Marls		−3.13	1.69	
Mean value of marls ($n = 3$)				−3.2±0.1	1.6±0.1	
Marly limestones associated with inoceramids						
ZU-11		Marly-limest.		−3.49	1.71	
ZU-1		Marly-limest.		−3.56	1.65	
Mean value of marly-limestones ($n = 2$)				−3.5±0.05	1.7±0.04	
BIDART SECTION						
Inoceramids						
Bid-18	Calcite	Marly-limest.	>1.5	−0.77	2.43	15.1
Bid-16	Calcite	Marly-limest.	>1.5	−0.86	1.74	15.5
Bid-13	Calcite	Marly-limest.	>3	−1.08	2.40	16.4
Bid-12	Calcite	Marly-limest.	>1	−0.74	1.82	14.9
Bid-10	Calcite	Marly-limest.	>1	−0.78	1.42	15.5
Bid-9	Calcite	Marl	>3	−0.70	1.79	15.1
Bid-7	Calcite	Marly-limest.	>1.5	−0.62	2.20	14.4
Bid-5	Calcite	Marl	>2	−0.65	2.14	14.5
Bid-4	Calcite	Marly-limest.	>2	−0.59	1.89	14.3
Bid-3	Calcite	Marly-limest.	>1	−0.63	2.30	14.5
Bid-2	Calcite	Marly-limest.	>1	−0.85	2.54	15.4
Bid-1	Calcite	Marly-limest.	>4	−0.38	2.01	13.4
Bid-1′(OSL)	Calcite	Marly-limest.	>4	−0.36	1.38	13.3
Bid-1′(MSL)	Calcite	Marly-limest.	>4	−0.32	1.54	13.1
Bid-1′(ISL)	Calcite	Marly-limest.	>4	−0.75	1.28	15.0
Bid-(-5)	Calcite	Marly-limest.	>2	−1.48	2.47	18.1
Mean value of inoceramids ($n = 16$)				−0.7±0.3	2.0±0.4	14.9
Marls associated with inoceramids						
Bid-9*		Marls		−1.36	1.84	
Bid-6		Marls		−1.69	1.80	
Bid-(-3)		Marls		−1.88	1.89	
Bid-(-6)		Marls		−2.15	2.47	
Mean value of marls ($n = 4$)				−1.8±0.3	2.00±0.3	
Marly limestones associated with inoceramids						
Bid-19		Marly-limest.		−1.25	2.21	
Bid-17		Marly-limest.		−1.65	1.91	
Bid-15		Marly-limest.		−1.39	1.92	
Bid-14		Marly-limest.		−1.54	1.92	
Bid-11		Marly-limest.		−1.47	1.93	
Bid-8		Marly-limest.		−2.20	1.98	
Bid-(-4)		Marly-limest.		−1.84	1.74	
Mean value of marly-limestones ($n = 7$)				−1.6±0.3	1.9±0.1	

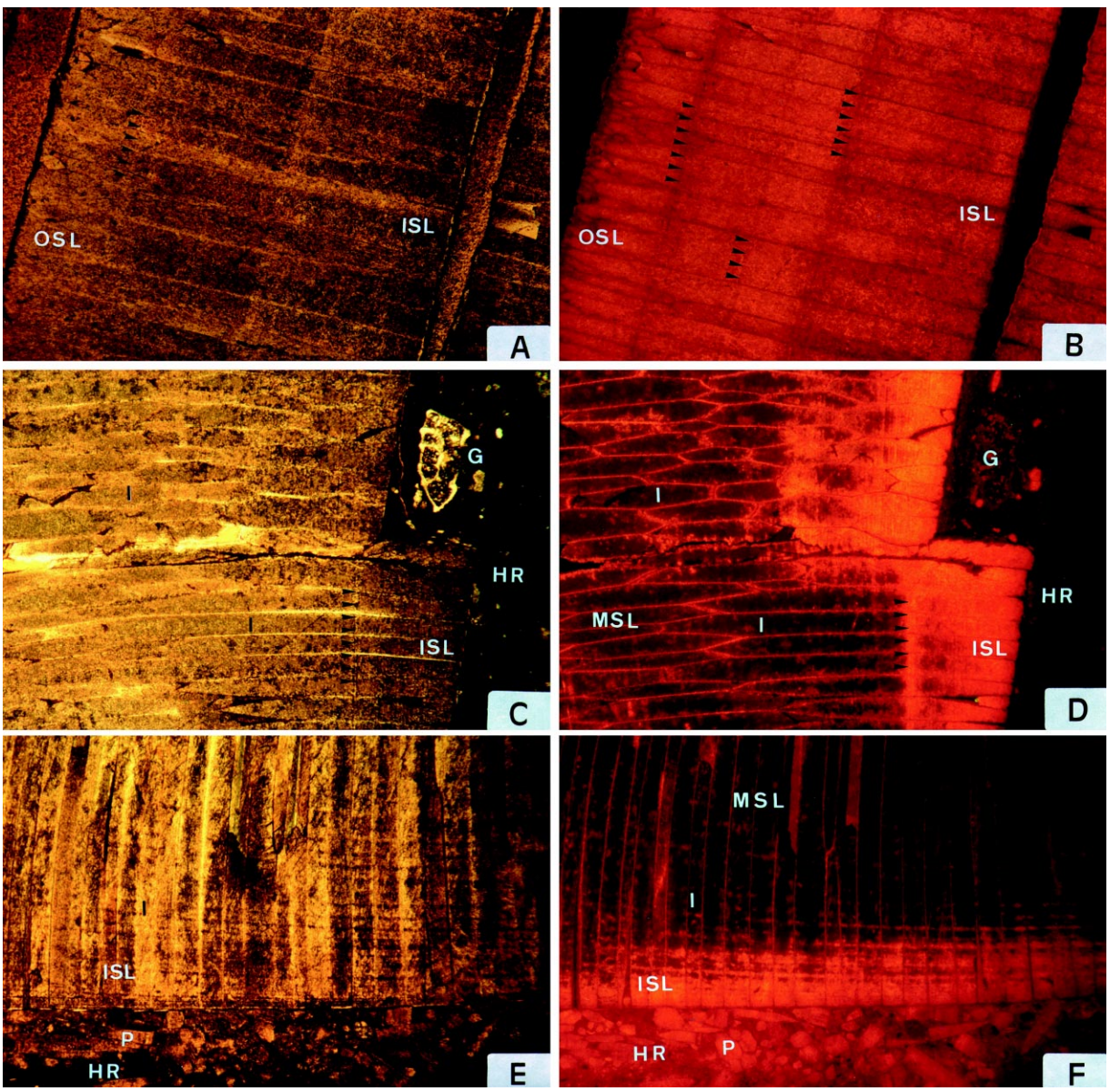

Fig. 4. Photomicrographs of inoceramid shells. (A) Prismatic microstructure view from the outer shell layer (*OSL*) to inner shell layer (*ISL*) of a complete inoceramid shell section. Weak growth lines, indicated by arrowheads, can be seen. ZU-15; Zumaya section. Photo width 2.6 mm. Plane-polarized light (PPL). (B) Cathodoluminescence (CL) image of (A), showing a homogeneous red–yellow luminescence. Growth lines are barely visible (arrowheads) and the smaller prisms of the outer shell layer (*OSL*) in comparison to the inner shell layer (*ISL*). (C) Prismatic microstructure of a fractured inoceramid shell (*I*) showing growth lines (arrowheads), near the inner shell layer (*ISL*). The micritic host-rock (*HR*) contains a globotruncanid section (*G*) infilled by sparry cement (sample BID-1; Bidart section). Photo width 2.6 mm (PPL). (D) The same image under CL, with brighter luminescence at the shell's edge. The CL colour grades from bright yellow/orange to dull red/brown toward the middle shell layer (*MSL*) and finally becomes non-luminescent. The joint lines between prisms (*I*) remain luminescent and it is interpreted to have functioned as paths for diagenetic fluids (see text). Both the host rock (*HR*) and the globotruncanid shell (*G*) are slightly luminescent. The calcite cement infilling the chambers can be distinguished. The fracture affecting the shell is clearly post-alteration (Bidart section). (E) An inoceramid shell showing a well-preserved prismatic microstructure (*I*) and moderately well-preserved growth lines in the inner shell layer (*ISL*). The host rock (*HR*) contains a lot of isolated prisms (*P*) and some foraminifera (BID-1, Bidart section). Photo width 2.6 mm (PPL). (F) CL image of photograph (A). Possible prior compositional control could explain the CL intensity of the growth lines and the gradual colouration from yellow-to-red-to-black from the inner shell layer (*ISL*) to the middle shell layer (*MSL*) (see text).

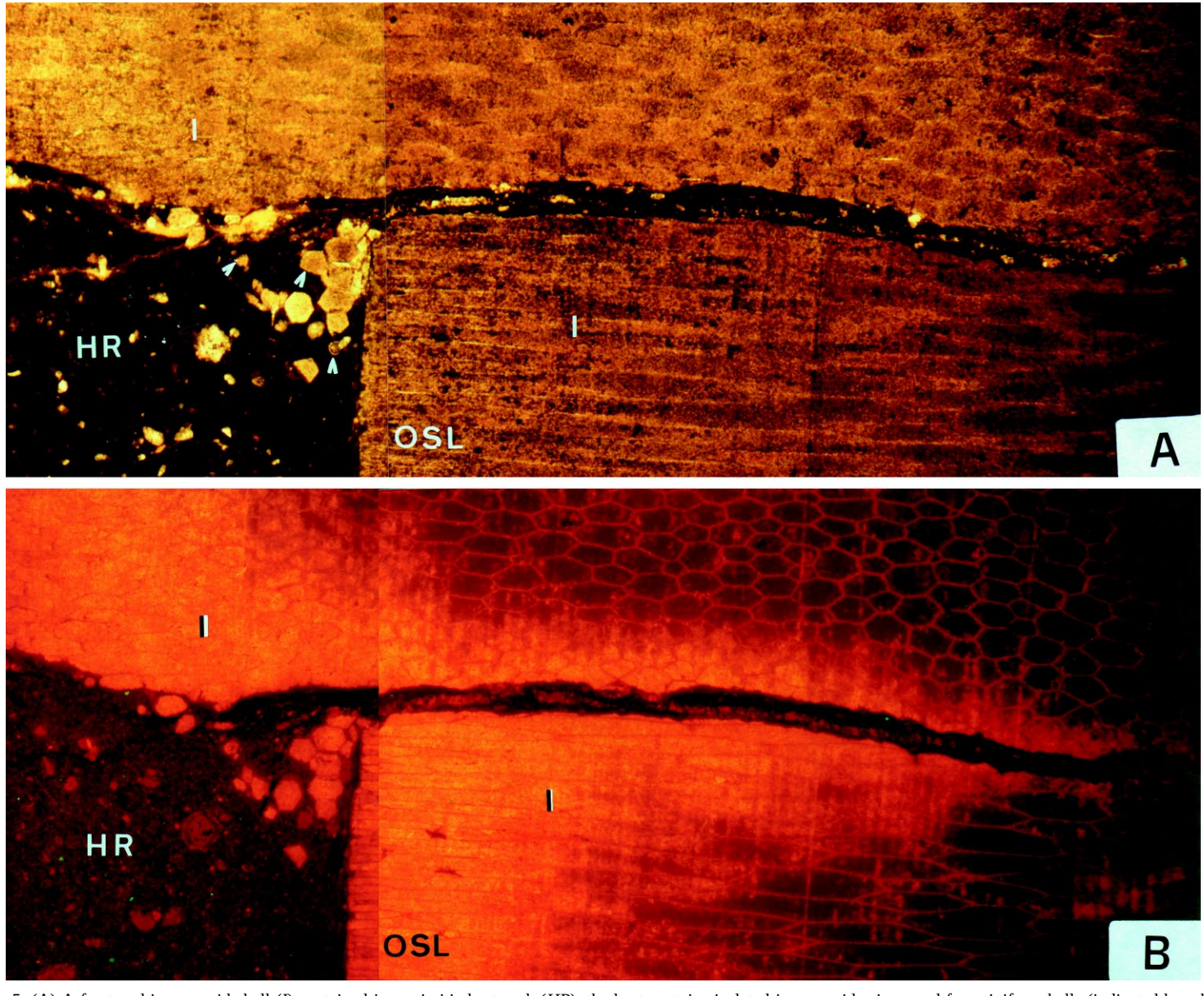

Fig. 5. (A) A fractured inoceramid shell (*I*) contained in a micritic host rock (*HR*); the host contains isolated inoceramid prisms and foraminifera shells (indicated by white arrowheads). The outer shell layer (*OSL*) is recognized by its small and thin prism network. Photo width 3.9 mm (PPL) (Bidart section). (B) CL image of (A) showing bright luminescence close to fracture planes with decreasing luminescence away from the fracture. The prism joints are luminescent as in previous examples. The orientation of the prisms is different in both parts, which suggests that in addition to a simple fracture, rotation has also occurred. The fracture was produced before diagenetic alteration.

lowish to red colour (Fig. 4B). However, in samples from the Bidart section, we observed brighter luminescence towards the shell/host rock interface and variable luminescence away from that region (Fig. 4D, F). In the middle shell layer (MSL) very thin brightly luminescent material occurs continuously along the prism boundaries and as discontinuous bands perpendicular and longitudinal to the prisms (Fig. 4D, F and Fig. 5B). Finally, the wackestone host-rock and the microfossils contained as foraminifers are dully luminescent, whereas individual inoceramid prisms are more brightly luminescent (Fig. 4D, F and Fig. 5B).

Under SEM, the calcite prismatic layers of the shells collected from the Bidart section seem to be well-preserved and without evidence of neomorphism (Fig. 6A). There is a clear reduction of prism length and size of prisms from the inner shell layer (ISL) to the outer shell layer (OSL) in longitudinal section. The ISL, perpendicular to the long axis of

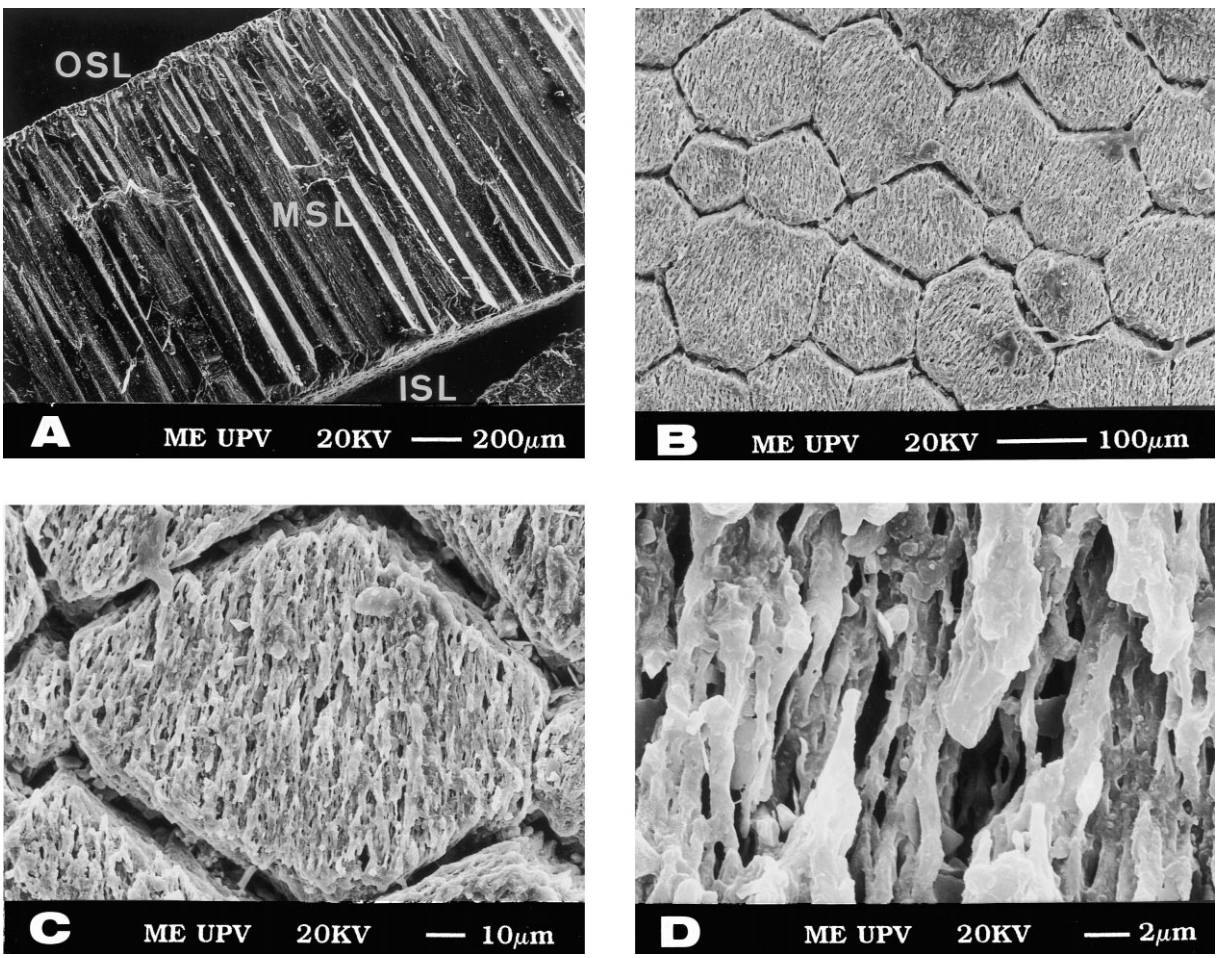

Fig. 6. Scanning electron photomicrographs of a non-etched, inoceramid shell from the Bidart section (BID-13_3). (A) A complete inoceramid section view from the inner shell layer (*ISL*) to the middle (*MSL*) and outer shell layers (*OSL*) showing that their calcitic prisms are not internally homogeneous. The number of prisms increases towards the OSL and they diminish in size. (B) A view of the ISL with characteristic polygonal, honeycomb morphology, illustrating the simple, prismatic calcite structure perpendicular to the long axis of the prisms with well-defined boundaries. (C) A close-up view of the inner shell layer showing long substructures with a well-oriented porosity, probably due to the disappearance of the organic matrix. (D) Details of the preceding photomicrograph. The regular porosity is almost free of diagenetic cement, such as calcite crystals due to minimum post-depositional alteration in this inner shell layer.

the prisms, is seen to consist of regular, simple prismatic calcite, with a polygonal honeycomb morphology and well-defined surface boundaries (Fig. 6B). The seemingly long granular substructure shows a uniformly distributed porosity, with different orientations among prisms (Fig. 6C). Under higher magnification (× 4300) this regular porosity can be seen to consist of ovoid pits, with very few calcite sheets as cement (Fig. 6D). The almost complete absence of calcite crystals as cement inside the pits could be interpreted as evidence of non-intense, diagenetic activity.

However, the microstructures observed in the ISL and the OSL of the inoceramid shells from the Sopelana and Zumaya sections are intensely modified. The polygonal honeycomb morphology of the ISL is maintained (Fig. 7A), with size and shape very similar to the microstructure described before from the Bidart section (Fig. 6A). Nevertheless, at higher magnification, we can appreciate badly defined limits among prisms and the absence of an uniformly distributed porosity (Fig. 7C) and the incorporation of substantial sheets of carbonate fill the ovoidal pits (Fig. 7E). The OSL shows surface prisms which are strongly diminished in size (Fig. 7B) (1/10 approximately) in comparison with the polygonal honeycomb morphology of the ISL (Fig. 7A). Evidence of a homogenized process with loss of surface boundaries by cementation is apparent (Fig. 7D, F). The diagenetic alteration undergone by these inoceramid shells is evident.

4.2. Oxygen and carbon isotopic data

The $\delta^{18}O$ and $\delta^{13}C$ values (in ‰ PDB) of 42 samples collected from the Sopelana section were determined (28 inoceramid shells; 6 marls; 8 marly limestones, see Table 1). The $\delta^{18}O$ values of the inoceramid shells vary from -5.18 to -2.94 and have a mean value of -3.6 ± 0.5; $\delta^{13}C$ values range from 1.32 to 2.53 with a mean value of 1.9 ± 0.3. The $\delta^{18}O$ values of marl range from -4.27 to -3.95, and have a mean value of -4.1 ± 0.1; $\delta^{13}C$ values of the marl range from 1.73 to 1.88, with a mean of 1.8 ± 0.05. The $\delta^{18}O$ values of the marly limestone range from -4.51 to -3.89, with a mean value of -4.1 ± 0.2; $\delta^{13}C$ values of the marly limestone range from 1.77 to 1.92, with a mean value of 1.8 ± 0.05. When $\delta^{18}O$ values are plotted against the $\delta^{13}C$ values, the resulting dots (inside the area X) lie outside the shaded LMC area (low magnesium calcite) (Fig. 8A). This rectangular shady field defines the lower and higher limits (0.0 to -2.0‰ $\delta^{18}O$; 0.00 to 4.0‰ $\delta^{13}C$‰) for calcium carbonate precipitated in isotopic equilibrium with the ambient seawater (Morrison and Brand, 1986). This indicates that they have undergone a clear diagenetic effect. Lithological types (marl and marly limestone) and the isotopic values/shell thickness ratio do not seem to be of significant importance in relation to the diagenesis (Fig. 8B, C).

A total of 16 samples from the Zumaya section were subject to $\delta^{18}O$ and $\delta^{13}C$ isotopic analysis (11 inoceramid shells; 3 marls; 2 marly limestones, see Table 1). The $\delta^{18}O$ values of inoceramid shells fluctuate from -4.71 to -1.88 with a mean value of -3.2 ± 0.7; $\delta^{13}C$ values range from 1.58 to 2.59 and have a mean value of 2.2 ± 0.3. The $\delta^{18}O$ values of marl samples vary from -3.30 to -3.13; $\delta^{13}C$ values of marl range from 1.58 to 1.69. The $\delta^{18}O$ values of marly limestone vary from -4.56 to -3.49; $\delta^{13}C$ values of marly limestone range from 1.65 to 1.71. The plotting of $\delta^{18}O$ against $\delta^{13}C$ reveals that all the samples of inoceramid shells (with the exception of ZU-13) lie outside the LMC stability field (Fig. 8A), thus suggesting diagenetic modification. Once again, the lithology and isotopic values/shell thickness ratio do not seem to be significant (Fig. 8B, C).

Fig. 7. Scanning electron photomicrographs of a non-etched inoceramid shell from the Sopelana section (MA-26). (A) A view of the ISL with characteristic polygonal, honeycomb morphology, illustrating the simple, prismatic calcite structure similar to Fig. 6B, but with evidence of a modified and compacted surface. Notice that the honeycomb boundaries are less well defined than in Fig. 6B. (B) View of the OSL, with the size of prisms clearly diminished. The prisms seem to be well cemented together. (C) View of a prism of (A). Note the different aspect in relation to Fig. 6B. (D) Part of (B), with several prisms interconnected by cement (*C*). Note that (A) and (B) have the same scale; the same for (C) and (D). (E) Detail of (C) showing the long substructures, similar to Fig. 6D, but progressively obliterated. The porosity, generated by the disappearance of organic proteinaceous sheaths is infilled by calcitic cement (*C*). (F) Detail of (D) showing three individual prisms with evidence of cementation (*C*).

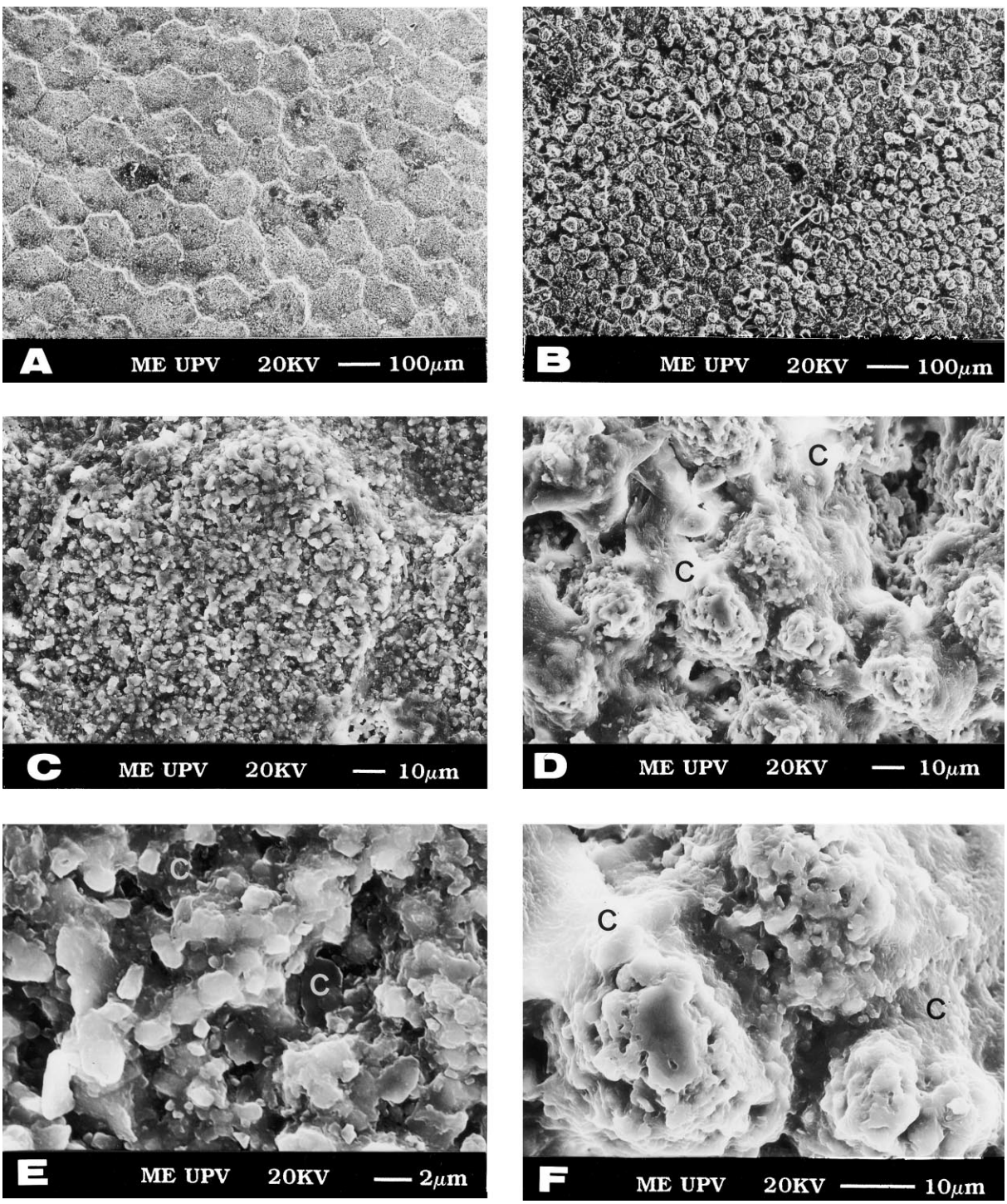
A ME UPV 20KV — 100μm
B ME UPV 20KV — 100μm
C ME UPV 20KV — 10μm
C
C
D ME UPV 20KV — 10μm
C
C
E ME UPV 20KV — 2μm
C
C
F ME UPV 20KV —— 10μm

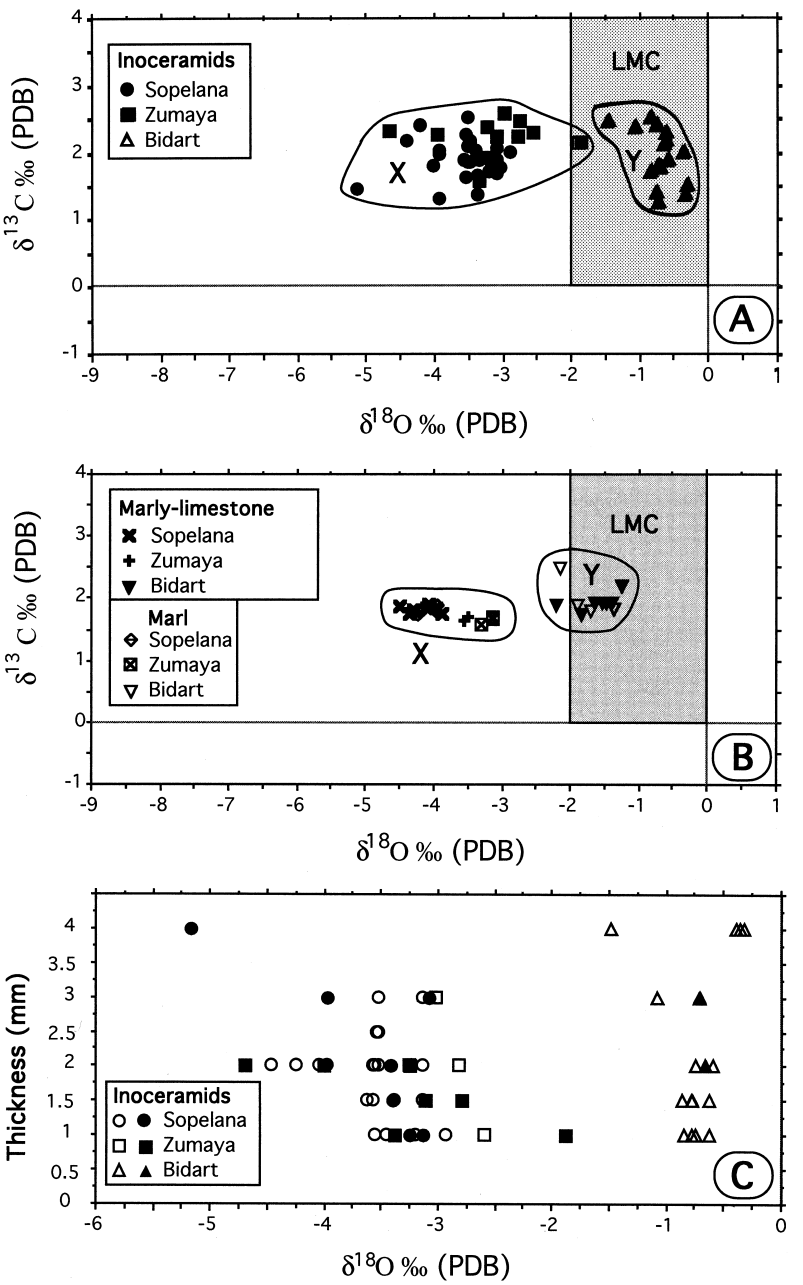

Fig. 8. (A) Carbon and oxygen isotope values from inoceramid shells from the sections Sopelana (28 samples), Zumaya (11 samples) and Bidart (16 samples). Two groups of dots can be seen: the group labelled *X* corresponds to the Sopelana and Zumaya specimens which are interpreted to have been affected by diagenesis; in the Bidart group (*Y*), the dots lie inside the LMC stability field for calcite precipitated in equilibrium with sea-water (Morrison and Brand, 1986). (B) The same trend is observed for marl and marly-limestone samples from Sopelana (6 and 8 samples, respectively), Zumaya (2 and 2) and Bidart (4 and 7). (C) Thickness of inoceramid shells with respect to the oxygen isotope value. No apparent trend is evident. Open symbols indicate inoceramids included in marly-limestone; solid symbols indicate inoceramids included in marl as host-rock.

Twenty-seven samples from the Bidart section were analyzed for $\delta^{18}O$ and $\delta^{13}C$ isotopic values (sixteen inoceramid shells, four marls, seven marly limestones, see Table 1). $\delta^{18}O$ values of shells range from -1.48 to -0.32 with a mean value of -0.7 ± 0.3; $\delta^{13}C$ values oscillate from 1.28 to 2.54 with a mean of 2.0 ± 0.4. $\delta^{18}O$ values of marl fluctuate from -2.15 to -1.36 with a mean of -1.8 ± 0.3; $\delta^{13}C$ values of the same samples range from 1.80 to 2.09 with a mean value of 1.9 ± 0.1. The $\delta^{18}O$ values of marly limestone vary from -2.20 to -1.25, with a mean value of -1.6 ± 0.3; $\delta^{13}C$ values of the same samples are from 1.74 to 2.21 and have a mean of 1.9 ± 0.1. Unlike the inoceramid samples from the former sections, the plot of $\delta^{18}O/\delta^{13}C$ shows that all data plot within the LMC stability field (Fig. 8A). This suggests that less diagenetic alteration occurred at Bidart in comparison to both the Zumaya or Sopelana sections, since diagenesis is supposed to deplete $\delta^{18}O$ values.

With a stainless-steel dental pick, three isotopic analyses were performed across one sample shell (Bid-1′). The diameter of each sampled spot was ~0.5 mm. The lightest oxygen values were recorded from the outer shell layer (Bid-1′OSL, −0.36‰ PDB) and the inner shell layer (Bid-1′ISL, −0.75‰ PDB), whereas the heaviest value was at the middle shell layer (Bid-1′MSL, −0.32‰ PDB) (Table 1).

In relation to the carbonate host-rock, with the exception of two samples (marl and marly-limestone), all the dots lie inside the LMC stability field. Once again, lithology and isotopic values/shell thickness ratios do not seem to play a significant role in the general diagenetic process (Fig. 8B, C).

4.3. Whole rock geochemistry

The occurrence of diagenetic alteration of inoceramid shells is also indicated by the depletion and enrichment of elements. We compared the concentrations of elements in: (1) the isotopically lightest inoceramid samples, and (2) the heaviest inoceramid samples. These values were related to the mean value of the whole host-rock (marl or marly-limestone) bearing the shells.

Two marl/marly-limestone samples (MA-37, $\delta^{18}O‰ = -4.23‰$; MA-4, $\delta^{18}O‰ = -4.51‰$) and two inoceramid shell samples (MA-33, $\delta^{18}O = -5.18‰$; MA-2, $\delta^{18}O‰ = -2.94‰$), from the Sopelana section, which are representative of samples with light and heavy isotopic values, respectively (Table 2) were analyzed by ICP and ICP–MS. Twenty one elements (major, minor and trace) and fourteen REE's were detected. We also established the ratio between the geochemical values of inoceramid shell and marl/marly limestone considering the value of the latter as 1 (Fig. 9A).

The marl sample (ZU-16, $\delta^{18}O‰ = -3.30‰$) and two inoceramid shell samples (ZU-15, $\delta^{18}O = -4.71‰$; ZU-13, $\delta^{18}O‰ = -1.88‰$) from the Zumaya section were analyzed following the same procedure as that used in Sopelana. These two inoceramid samples have the lightest and heaviest isotopic values (Table 2). The ratio between geochemical values of inoceramid samples and marl (ZU-16 sample) was also established considering the value of the latter as 1 (Fig. 9B).

The marly limestone sample BID-14 and two samples of inoceramid shells (BID-(-5); $\delta^{18}O‰ = -1.48‰$ and BID-1; $\delta^{18}O‰ = -0.38‰$) from the Bidart section were analyzed by using a procedure similar to that employed in the former sections. These samples were selected since BID-(-5) has the lightest isotopic values, whereas BID-1 has the heaviest value (Table 2). The ratio between geochemical values of inoceramid shells and marly limestone was also established, considering the value of the latter as 1 (Fig. 9C).

4.4. Inoceramid shell chemistry by electronic microprobe

A total of 50 analyses were performed on samples from the Sopelana section to determine the Fe, Mn, Na, Sr and Mg contents in five different zones across the shell: (1) the outer shell layer (OSL); (2) the middle outer; (3) the middle shell layer (MSL); (4) the middle inner; and (5) the inner shell layer (ISL). In a similar manner, we carried out 55 analyses on samples from the Zumaya section and 55 analyses on samples from the Bidart section (Table 3 and Fig. 10). The Na content varies depending on the bands; it is low in the Sopelana and Zumaya samples, but may reach 1500 ppm in the first band and go down to 883 ppm in the fifth band. Sr maintains constant values in the Sopelana samples, but the Sr content increases in the

Table 2
Summary of the geochemical analyses of major, minor, traces and REE's elements for inoceramid shells (most and least diagenetically altered), marl or marly-limestones from the Sopelana, Zumaya and Bidart sections (detection limits are included together with the elements in wt% or in ppm)

Sections:	Sopelana section				Zumaya section			Bidart section		
Sample:	MA-37	MA-4	MA-33	MA-2	ZU-16	ZU-13	ZU-15	BID-14	BID-(-5)	BID-1
Rock/Fossil:	Marl	Marly-lim.	Inoc.	Inoc.	Marl	Inoc.	Inoc.	Marly-lim.	Inoc.	Inoc.
$\delta^{18}O$	−4.23	−4.51	−5.18	−2.94	−3.3	−1.88	−4.71	−1.54	−1.48	−0.38
Na_2O (0.05%)	0.53	0.37	0.08	0.09	0.69	0.05	0.11	0.29	0.21	0.04
Rb (0.50 ppm)	88.6	56.9	6.2	3.83	112	0.58	2.55	76.6	4.52	0.73
CaO (0.05%)	31.43	40.16	50.76	52.93	28.7	51.22	48.25	37.08	50.76	51.16
Ba (0.50 ppm)	207	137	19.7	14.1	233	91.8	85.7	147	14	5.96
Sr (2.00 ppm)	836	900	880	1,264	950	1,338	1,370	804	1,048	1,131
V (2.00 ppm)	61.1	40.9	4.77	4.73	75.2	2.28	4.09	54.1	8.77	2.03
Nb (0.50 ppm)	7.24	4.19	0.31	0.3	7.84	0.08	0.36	5.38	0.42	0.12
Zr (2.00 ppm)	90.7	43.7	5.45	7.14	75.6	1.26	2.3	48.7	3.91	7.34
MgO (0.05%)	0.81	0.62	0.68	0.7	1.06	0.65	0.64	0.75	0.79	1.06
Fe_2O_3 (0.10%)	2.19	1.56	0.37	0.29	3.18	0.36	0.74	2.16	0.34	0.15
MnO (0.01%)	0.04	0.07	0.06	0.08	0.04	0.07	0.05	0.06	0.1	0
Cr (1.00 ppm)	43	28.8	4.92	5.02	52.8	3.55	3.41	36.7	5.92	2.51
Co (1.00 ppm)	11.1	13.9	1.71	1.87	8.27	0.7	0.73	15.2	1.8	0.42
Cu (1.00 ppm)	15.8	12.8	13.2	11.7	19.4	7.25	405	12.2	47.2	79.9
Ni (1.00 ppm)	25.4	17.5	9.54	17.6	30.5	18	14.2	23.3	10.1	13.2
Zn (2.00 ppm)	70.4	30.4	12.9	15.1	58.3	7.89	8.72	42.3	14	9.98
P_2O_5 (0.05%)	0.16	0.06	0.02	0	0.06	0.02	0	0.07	0.02	0
Al_2O_3 (0.10%)	8.15	5.44	0.51	0.33	9.72	0.08	0.54	7.1	0.42	0.07
SiO_2 (0.20%)	26.11	16.58	1.4	0.94	28.21	0.28	1.46	17.85	1.04	0.18
Y (0.10 ppm)	12.8	11.4	4.37	5.37	16.9	3.42	13.2	11.9	3.61	1.84
La (0.10 ppm)	17.63	12.45	3.66	4.43	22.14	2.23	6.54	14.5	3.2	1.308
Ce (0.10 ppm)	30.99	21.71	5.27	5.101	41.64	3.06	16.37	25.36	4	1.195
Pr (0.03 ppm)	3.83	2.81	0.74	0.773	5.01	0.48	1.86	3.13	0.62	0.22
Nd (0.10 ppm)	15.39	11.01	3.19	3.063	19.41	1.85	8.26	12.16	2.51	0.88
Sm (0.10 ppm)	3.09	2.32	0.67	0.569	3.88	0.4	2.06	2.27	0.5	0.133
Eu (0.01 ppm)	0.57	0.46	0.17	0.155	0.85	0.1	0.435	0.44	0.13	0.045
Gd (0.10 ppm)	2.38	1.87	0.55	0.692	3.42	0.38	1.957	2.08	0.46	0.198
Tb (0.03 ppm)	0.36	0.29	0.09	0.096	0.51	0.07	0.318	0.31	0.07	0.03
Dy (0.10 ppm)	2.2	1.75	0.61	0.609	2.93	0.41	1.876	1.71	0.46	0.168
Ho (0.03 ppm)	0.47	0.37	0.14	0.146	0.67	0.11	0.474	0.4	0.1	0.045
Er (0.10 ppm)	1.2	0.94	0.34	0.347	1.573	0.23	1.233	1.03	0.28	0.12
Tm (0.03 ppm)	0.17	0.12	0.05	0.066	0.254	0.03	0.189	0.15	0.05	0.018
Yb (0.10 ppm)	1.22	0.84	0.41	0.406	1.7	0.24	1.32	1.1	0.31	0.111
Lu (0.01 ppm)	0.19	0.13	0.05	0.061	0.241	0.04	0.177	0.17	0.05	0.019
Sc (ppm)	11.3	10.3	6.6	6.4	11.1	4.1	9.1	11.1	7.4	4

2nd, 3rd and 4th bands of the Zumaya samples. The Sr content in the Bidart samples ranges from 1015 ppm (1st band) to 2500 ppm (5th band). The Mg content tends to diminish from the external to the internal shell bands in the samples taken from Sopelana. The Mg evolution in the Zumaya samples is uncertain, whereas in the Bidart specimens the Mg content is higher in the 3rd and 4th bands. The chemical composition of inoceramid shells in mole percent ($CaCO_3$ mol% + $MgCO_3$ mol% + (Fe + Mn)CO_3 mol%) shows that all the samples are composed of low-magnesium calcite (LMC with <4 mol% $MgCO_3$), with mean values ranging from 1.4 to 2.9 mol% $MgCO_3$. Only the second band in the Sopelana samples has a higher value (4.3 mol% $MgCO_3$), without any clear reason being evident (Table 3).

5. Discussion

5.1. Diagenetic evidence

Cathodoluminescence reveals several patterns indicative of diagenetic alteration. On the one hand, inoceramid shells from the Sopelana and Zumaya sections show very homogeneous red to yellowish colours, the latter occurring in the most altered zones. The paths for diagenetic fluids are almost completely obliterated (Fig. 4A, B).

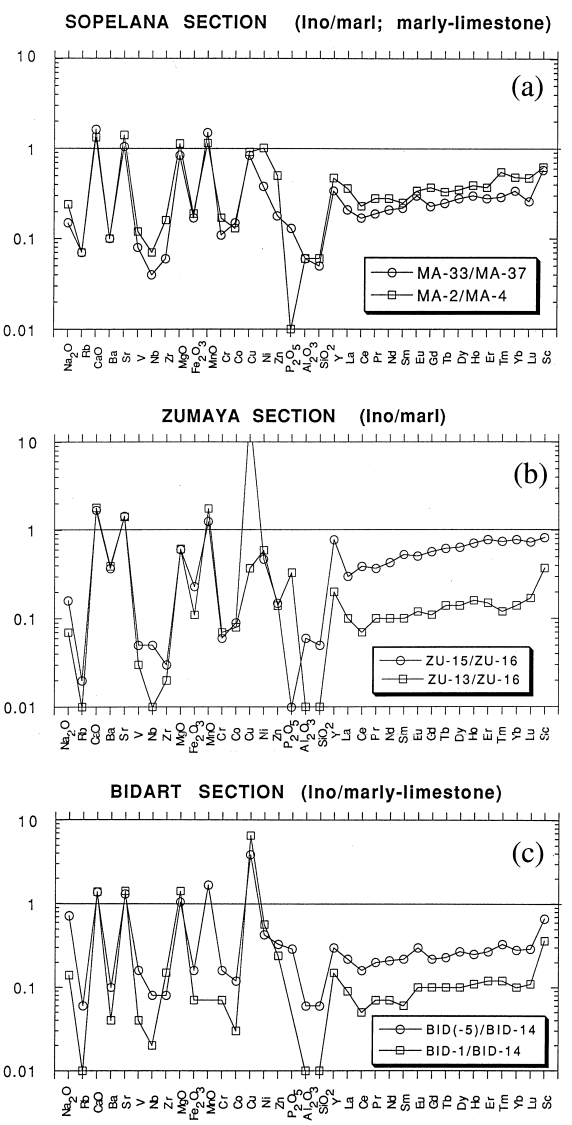

However, the diagenetic process preserved the biological growth lines, which appear homogeneous and sometimes recognizable under CL as an alternation of luminescent and non-luminescent bands. As early as 1979, Ragland et al. (1979) detected diagenetic changes before recrystallization and significant variations in the Mg, Sr, Mn, Na and K contents of unrecrystallized gastropod and bivalve shells from the Late Cretaceous to Holocene, in several areas on the southeastern U.S. Atlantic Continental Shelf. A similar type of diagenesis may have affected the inoceramid shells from the Bidart section. The wackestone host-rock is poorly luminescent, probably due to its MnO content (0.04–0.07%), which in turn is very similar to that of the inoceramid shell (0.06–0.08%) as observed in the Sopelana and Zumaya sections. Stronger variations between the host-rock (0.06%) and inoceramid shell (0.1 to 0%) occurred in the Bidart section (Table 2).

On the other hand, samples from the less-diagenetized Bidart section provide clearer evidence of diagenetic advance mechanisms:

(a) The OSL is yellow, whereas the MSL shows a well-preserved prism arrangement yielding a zonation from red to non-luminescent just at the middle zone (Fig. 4C, D).

(b) The diagenetic fluid advance lines are red-luminescent and, with the exception of fractures, fully coincide with the thin boundaries between non-

Fig. 9. Analytical results of the most and the least diagenetically altered (as defined by $\delta^{18}O$) inoceramid shells versus the whole rock (marl or marly-limestone). (A) Inoceramid shells (MA-33; $\delta^{18}O = -5.18‰$ PDB) and (MA-2; $\delta^{18}O = -2.94‰$ PDB) versus the whole rock (MA-37; $\delta^{18}O = -4.23‰$ PDB) and (MA-4; $\delta^{18}O = -4.51‰$ PDB), in the Sopelana section. (B) The same relation applied to the inoceramid shells from the Zumaya section (ZU-15; $\delta^{18}O = -4.71‰$ PDB) and (ZU-13; $\delta^{18}O = -1.88‰$PDB) versus the whole rock (ZU-16; $\delta^{18}O = -3.30‰$ PDB). (C) The same relation in the Bidart section inoceramid shells (BID-(-5), $\delta^{18}O = -1.48‰$ PDB; BID-1, $\delta^{18}O = -0.38‰$ PDB) and their corresponding marly-limestone (BID-14; $\delta^{18}O = -1.54‰$ PDB). The REE relations are very sensitive to diagenesis, and those of the most diagenetized shells are close to those of the host rock, as can be seen in the Zumaya and Bidart sections. In the Sopelana section, a contrary trend is observed, which can be explained in terms of the different wealth and mobility of REEs inside marl or marly-limestone deposits. *Ino/marl* = inoceramid value/marl value.

Table 3
Summary of geochemical mean values for inoceramid shells (1st to 5th band) in ppm and mol% of the Sopelana, Zumaya and Bidart sections

	Inoceramid shell, 1st band			Inoceramid shell, 2nd band			Inoceramid shell, 3rd band			Inoceramid shell, 4th band			Inoceramid shell, 5th band		
Sections Mean values	Sopelana $n = 10$	Zumaya $n = 11$	Bidart $n = 11$	Sopelana $n = 10$	Zumaya $n = 11$	Bidart $n = 11$	Sopelana $n = 10$	Zumaya $n = 11$	Bidart $n = 11$	Sopelana $n = 10$	Zumaya $n = 11$	Bidart $n = 11$	Sopelana $n = 10$	Zumaya $n = 11$	Bidart $n = 11$
Sr (ppm)	693	998	1015	837	827	1115	786	1226	1553	879	2001	2345	1049	987	2498
Fe (ppm)	3692	3709	2502	801	2173	2954	1609	2256	1844	1803	1803	551	3234	3985	1449
Mn (ppm)	1510	1006	1169	364	693	1119	287	645	366	651	713	225	1317	998	1197
Mg (ppm)	6818	3481	5017	10920	4272	4178	5676	4005	6229	5441	4911	6887	3474	4506	5001
Na (ppm)	267	257	1409	682	117	1180	437	349	1065	111	292	1119	556	387	883
$CaCO_3$ mol%	96.5	97.8	97.2	95.5	97.8	97.6	97.4	97.9	97	97.5	97.5	97	97.8	97.3	97.4
$MgCO_3$ mol%	2.6	1.4	2.1	4.3	1.7	1.7	2.3	1.6	2.6	2.1	2	2.9	1.4	1.8	2.1
Sid.% + Rod.%	0.9	0.8	0.7	0.2	0.5	0.7	0.3	0.5	0.4	0.4	0.5	0.1	0.8	0.9	0.5

The shell mineralogy is clearly low-magnesium calcite (LMC <4 mol% $MgCO_3$).

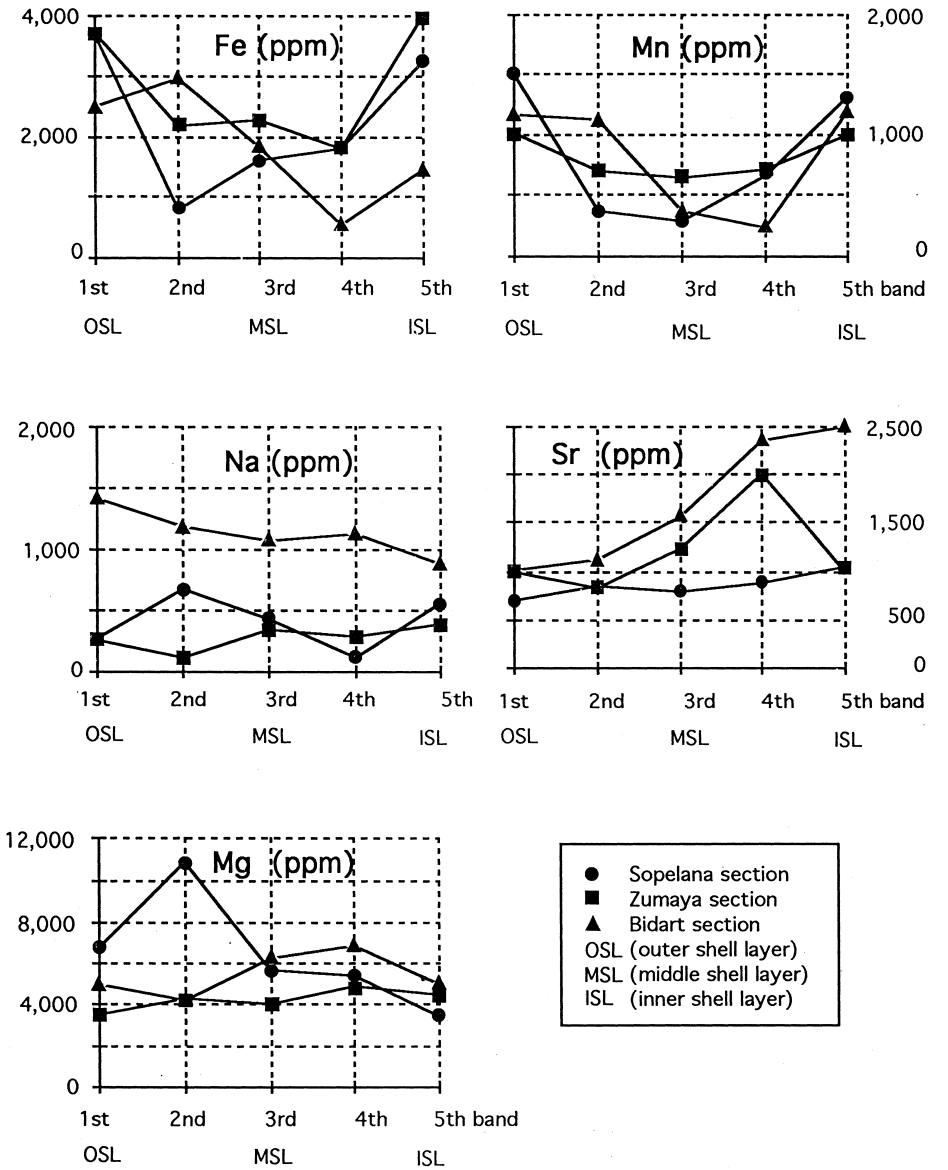

Fig. 10. Fe, Mn, Na, Sr and Mg values in ppm were analyzed across five bands (from OSL to ISL) of inoceramid shells from the Sopelana, Zumaya and Bidart sections. The Fe and Mn are lowest closest to the central area, while the Na and Mg fluctuate and do not show a clear trend. Sr content has its maximum value in the 5th band of samples from the least diagenetically altered area of the Bidart section.

disintegrated prisms. Such boundaries could have harboured a large proteic content (Fig. 4D).

(c) The natural growth lines of the shells controlled the advance of diagenetic fluids and sometimes acted as chemical barriers (Fig. 4E, F). An alternation of red–yellowish–black luminescent colours appears along the growth lines. This observation can be interpreted in two ways: (1) colour zoning could reflect compositional differences caused by original biological growth, without an important cationic modification by diagenesis; or (2) colour zoning could reflect diagenetic alteration focused along growth lines (Fig. 4E, F). In our opinion, the second explanation is favoured, since the pattern is

best observed near the interface with the carbonate host-rock. Away from this contact, growth lines are visible in plain light but not CL. Luminescent alternation only appears in the outer or inner parts of the shell, but not in the middle in which the growth lines are non-luminescent or weakly red luminescent, as can be observed in Fig. 4B.

(d) The isolated prisms detached from the shell and surrounded by sediment exhibit a luminescent yellow colour. These isolated prisms could be more easily altered than intact shell (Fig. 4F).

(e) Since luminescent joints between prisms are broken, we believe that fracturing and packing of shells occurred after early diagenesis (Fig. 4D). Major fractures seem to have formed prior to diagenetic alteration and may have functioned as paths for diagenetic fluids (Fig. 5A, B) since shell material near these breaks luminesce brightly. Nevertheless other fractures (Fig. 4D), cut luminescent bands and seem to post-date alteration.

These peculiarities observed using CL are confirmed under SEM. In the inoceramid shell samples of the Bidart section, the ISL has a well-developed, polygonal honeycomb morphology with a uniformly distributed porosity and cementation is almost absence (Fig. 6). The ovoidal pits may originate from the breakdown of organic matrix. The admittedly high concentration of proteic matrix interspersed among the mineral structure could endow the inoceramid shells with a degree of flexibility necessary in deep waters. On the contrary, the OSL and ISL of the inoceramid shell samples from the Zumaya section present a diagenetically altered morphology with the original microstructure substantially modified by an intense cementation process described above (Fig. 7).

With regard to the Sopelana and Zumaya series, the mean oxygen isotopic values of inoceramid shells are clearly lighter (−3.6 ‰ in Sopelana, −3.2‰ PDB in Zumaya) than those found at Bidart (−0.72‰ PDB). The same tendency is observed for the mean values of marls (−4.1‰ PDB in Sopelana, −3.2‰ in Zumaya, −1.8‰ in Bidart) and marly limestones (−4.1‰, −3.5‰ and −1.6‰ PDB, respectively) (Fig. 8A, B). For this reason, inoceramid shells, marls and marly limestones from the Bidart section, which have the highest oxygen isotopic values, are less affected by diagenesis and the palaeotemperatures estimated from the inoceramid shells of the Bidart section deposits can be considered as being most representative of the palaeoenvironmental conditions during the mid-Maastrichtian at the Basque Arc. The palaeotemperatures estimated from the inoceramid shells of the Sopelana and Zumaya sections have been rejected.

Nevertheless, the data which most clearly indicate the post-depositional diagenetic evolution undergone by the LMC prisms of the inoceramid samples from the Sopelana, Zumaya and Bidart sections is the content of minor and trace elements and REE's in the whole-rock and inoceramid shells, together with the Sr, Mg, Na, Fe, and Mn values measured across the five bands of the shells (Fig. 9A, B, C, Table 2).

The inoceramid shell/host rock (IS/HR) ratios for minor and trace elements and REE's are quite significant. In the Zumaya and Bidart sections, the IS/HR ratio for minor and trace elements and REE's tends to be close to unity. The closer to 1 the IS/HR ratio is, the higher the diagenetic degree becomes. As shown in Fig. 9B and C, the IS/HR ratio of samples ZU-15/ZU16 and BID(-5)/BID-14, which are the most altered diagenetically, are closer to 1, unlike the least diagenetically altered samples ZU-13/ZU-16 and BID-1/BID-14. The REE values better indicate this trend in spite of their low ppm values. This same tendency (IS/HR) was observed in different places from the Basque Arc, such as in the Barrika section (Elorza and García-Garmilla, 1996).

The Sopelana samples deserve some additional comments. Contrary to what may be expected, the IS/HR is far from 1 in the more diagenetically altered material (MA-33/MA-37), in comparison to the less diagenetically altered MA-2/MA-4, in which the IS/HR is closer to 1 (Fig. 9A). We suggest that despite the fact that shell MA-33 has light isotopic values ($\delta^{18}O = -5.18$‰ vs. PDB) and the marl (MA-37) is enriched with potentially interchangeable elements, the mobilization of cations that should have been absorbed by the shells was inhibited since the permeability of the marl may have been relatively low in comparison to that of the marly limestone (MA-4). Analysis of additional samples from this area will facilitate our testing of this hypothesis. This may explain why the inoceramid shells contained in porous limestone host rocks are enriched in elements of the latter, whereas the shells

included in marls are poor in elements supplied from the marly host rock.

The analyses of the shells across the five bands under the electronic microprobe show a symptomatic evolution in Fe and Mn with minimum values in the central bands (Fig. 10), and indicate an important and similar input in the outer and inner surfaces of the shell, which is clearly diagenetic in the Sopelana and Zumaya sections. Fe values of samples taken from Bidart do not follow this trend, probably owing to a lower degree of diagenesis. This can be explained by the natural enrichment in Mg just at the inner part (3th and 4th band) of the shell, an element which has been replaced by cations such as Mn and Fe at the edges.

As Fig. 10 and Table 3 show, the evolution of cationic contents across the shell is, in general, gradual, with excursions due only to the biological growth. Fe and Mn are more abundant just at the shell edges. The higher the Na and Sr contents, the lighter the diagenetic alteration. Finally, Mg seems to be concentrated in the central part of the less diagenetically altered shells.

5.2. Palaeoenvironmental implications

The 'vital effect' typically gives rise to lighter rather than heavier $\delta^{13}C$ values with a variable intake of isotopically light metabolic CO_2 into the skeletal carbonate (Pirrie and Marshall, 1990a), whereas the removal of CO_2 by photosynthesis causes heavier carbon values in carbonates (Marshall, 1992). This outwardly simple tendency could be modified by the presence of symbiotic bacteria known to highly fractionate carbon isotope values of the outer layer during mollusc shell growth. Rio et al. (1992) confirm that the mean $\delta^{13}C$ values of present-day bivalve shells living near the hydrothermal vent of the East Pacific Rise or near oceanic cold seeps (Florida, Louisiana, Oregon, Japan) are generally different from those of normal marine shells. If they live with methane-oxidizing bacteria they are ^{13}C-depleted, and when they contain sulphide-oxidizing bacteria they can be ^{13}C-enriched.

The mean carbon isotope values are rather constant across sample type at Bidart (2.0‰ PDB inoceramid shells, 2.0‰ marls and 1.9‰ marly-limestones), which suggests the absence of a substantial 'vital effect' upon inoceramid shells. More disperse values are observed in the Sopelana samples (1.9‰, 1.8‰ and 1.8‰, respectively), as well as in those from Zumaya (2.2‰, 1.6‰ and 1.7‰, respectively). The Zumaya mean value (2.2‰) differs from that of Sopelana and Bidart owing to environmental factors, such as a strong siliciclastic input, as mentioned in Mount and Ward (1986).

When the equation of Craig (1965) is applied to the Bidart oxygen isotope values, the mean palaeotemperature obtained from inoceramid shells is close to 15ºC, with a minimum of 13.1ºC and a maximum of 18.1ºC (Table 1). As has been mentioned before, three isotopic analyses were performed across the shell in one sample (Bid-1′). The lightest oxygen values were recorded from the outer shell layer (Bid-1′OSL)(−0.36‰ PDB) and the inner shell layer (Bid-1′ISL) (−0.75‰ PDB), whereas the heaviest value was at the middle shell layer (Bid-1′MSL) (−0.32‰ PDB). The latter value suggests a palaeotemperature of 13ºC, perhaps relatively close to that of marine bottom water, because the internal part of the shell is non-luminescent and presumably less diagenetically altered.

Clauser (1994) estimated for the Bidart section 24ºC for the lower Campanian–lower Maastrichtian and 18ºC for the upper Campanian and upper Maastrichtian at 30ºN. These palaeotemperatures were determined from $\delta^{18}O$‰(PDB) values of marls and marly-limestones. The values of both lithologic types are very similar (from −2.2‰ PDB to −1.2‰) and a mean value of −1.5‰ was obtained by Clauser (op. cit.) in the zone running from the maximum development of inoceramids up to their disappearance (section 14, lithology 3). This author claimed that the development of icecaps could have started during Maastrichtian times at latitude 80ºN and at temperatures of 3ºC and 1ºC for the lower and upper Maastrichtian, respectively. We have measured in the same zone mean values of −1.8‰ and −1.6‰ PDB for marls and marly-limestones, respectively (Table 1). Our results are slightly different from the mean value of −1.5‰ PDB obtained by Clauser (1994), and are in our opinion undoubtedly indicative of mixed planktonic and benthonic microfaunas, together with a diagenetic cementation and tectonic fabric, from which it is inadvisable to deduce an oceanic water palaeotemperature.

A general cooling trend is assumed in marine waters from the Cenomanian to the Maastrichtian (Barrera et al., 1987; Pirrie and Marshall, 1990b; Barrera, 1994; Jenkyns et al., 1994; Ditchfield et al., 1994). In northern Morocco, Lécuyer et al. (1993) based on variations in $\delta^{18}O‰$ values of well preserved phosphatic teeth (shark and ray) recorded substantial features about thermal variations within the water column of the western Tethys. In this way, tropical waters with a mean temperature of 27ºC underwent rapid cooling down to about 19ºC in the early Maastrichtian, followed by a period of consistently low temperatures. The faunas collected in Morocco correspond to nektonic and benthic associations and the calculated water depth did not exceed 200 m. This mean value of about 19ºC is consistent with our lower palaeotemperature value of 13ºC when the higher latitude (30ºN) assigned for the Bidart section (Clauser, 1994).

From Cretaceous northwest European chalk shelf deposits a cooling trend along the Upper Cretaceous (Jenkyns et al., 1994) and a particular cooling from the upper Campanian to lower Maastrichtian have been detected (Schönfeld et al., 1991). In northern Belgium, Elorza et al. (1997) deduced from less diagenetically altered belemnites mean palaeotemperatures of 12.5ºC for the late Campanian and 11.3ºC for the early Maastrichtian, whereas the temperature values obtained from diagenetically altered inoceramids (13.9ºC and 24.1ºC, respectively) cannot be taken into consideration for palaeoenvironmental interpretations.

Temperatures closer to 10–11ºC were estimated by Barrera and Huber (1990) for the early Maastrichtian, whereas during the late Maastrichtian, the water temperature could have been close to 9ºC in the Maud Rise (South Atlantic region, ODP Sites 689 and 690 at latitude 65ºS). These palaeotemperatures are based on the isotopic relations in *Gavelinella beccariiformis* and indicate that bottom waters (at a depth of about 1500 m) in the southern South Atlantic were probably of an Antarctic origin. On the other hand, Barrera et al. (1987) estimated 5.5ºC to 9ºC for the Seymour Island (Antarctic Peninsula) shelf bottom-water during the early Maastrichtian and 4º to 8.5ºC for the late Maastrichtian. Boersma (1984) calculated a temperature of 9ºC for intermediate waters in the Agulhas Plateau during the latest Maastrichtian based on different analyses on *G. beccariiformis*. Shackleton et al. (1984) inferred temperatures from 6.5ºC to 10ºC for sites 525 and 527 in the South Atlantic, based on benthic data.

5.3. Inoceramid extinction

Except for the enigmatic *Tenuipteria argentea* (Conrad) form which occurs at low abundances throughout the upper Maastrichtian, it is admitted, at least in the Basque Cantabrian region, that the bivalve family Inoceramidae declined gradually in both abundance and species diversity over tens of metres of stratigraphic section; the last species disappeared between 2 and 2.5 m.y. before the K/T boundary, just when the *Gansserina gansseri* planktonic foraminiferal biozone vertically evolved to the *Abathomphalus mayaroensis* zone (MacLeod and Hoppe, 1992; MacLeod, 1994).

Different authors have proposed opposing ideas to explain inoceramid extinction, particularly as regards the temperature of oceanic waters. It has been suggested that the pattern and timing of inoceramid extinction reflects a worldwide phenomenon and may be part of a mid-Maastrichtian event that was global in extent (D'Hondt, 1983; Ward et al., 1991; MacLeod and Hoppe, 1992; MacLeod, 1994). Another hypothesis suggests that it was caused by warm episodic events related to decreasing of upwelling currents and primary productivity. This is supported by synchronic negative excursions of $\delta^{18}O‰$ PDB and $\delta^{13}C‰$ PDB (up to 2‰ PDB units) such as those of the Zumaya section, detected by Mount et al. (1986), just at the moment when marls begin to dominate marly-limestones. The oxygen isotope values obtained in Zumaya (Mount et al., 1986 and in this work) do not represent absolute original palaeotemperatures, but relative temperature changes since diagenesis complicates the interpretation of isotopic variations. Later, Margolis et al. (1987), based on substantial isotopic data from Upper Cretaceous and Lower Tertiary limestones and marlstones from the Zumaya section, considered that the ammonite and inoceramid disappearance coincides with two distinct episodes of negative carbon isotope excursions, which may reflect localized palaeoceanographic or ecological changes.

MacLeod (1994) and MacLeod et al. (1996) suggested that the decline in inoceramid abundance

corresponds to a major ecological event, which occurred over a resolvable interval of geological time, at different times, in different areas. Thus, an input of oxygen-rich, deep Antarctic waters during the Maastrichtian would have largely removed anoxic soft-bottom conditions, with a decrease in temperature. In fact, $^{18}O/^{16}O$ data suggest that Antarctic bottom waters were largely remobilized during the Campanian/Maastrichtian (Saltzman and Barron, 1982; Barron et al., 1984) and the waters became colder during the mid-Maastrichtian (Barrera and Huber, 1990; Thomas, 1990; Huber, 1990). Wang et al. (1986) and Hu et al. (1988) believe that the variations in the relative abundance of Ce at the beginning of the Campanian may reflect changes in the degree of oxygenation in bottom waters in the South Atlantic, which would account for inoceramid disappearance in deep waters.

Crame et al. (1996) and Crame and Luther (1997) determined within the James Ross Basin (Antarctica) that the stratigraphically highest molluscan macrofossils, such as a giant inoceramid bivalve, are dated as mid–late-Campanian, whereas belemnites correspond to early–mid-Campanian. The inoceramid shells are totally absent throughout the Maastrichtian succession. The evolution towards a giant size was interpreted as an antipredatory device, but the secretion of such large calcite shells may have become physiologically impractical when the seawater temperatures in the southern high latitudes were beginning to fall. Their mid- to late-Campanian extinction in Antarctica is exceptionally early and may be taken as a response to the regional shallowing event and a phase of high-latitude cooling.

The inoceramid shell isotope values we have obtained do not show a clear trend towards a decrease in temperature (Table 1), because the samples selected are prior to the decline in inoceramid abundance at the Sopelana and the Zumaya sections. Neither a decrease is detected in the thickness of the inoceramid shell along the stratigraphic sections that could suggest a calcite secretion crisis and an initial cooling. The inoceramid shell isotope values taken along the stratigraphic column of the Bidart section are very similar (Fig. 2). On the contrary, the lithologic contact with red marls already without inoceramids (Member III of MacLeod, 1994; Section 13, lithologic unit 6 of Clauser, 1994) marks a negative excursion of $\delta^{18}O‰$ (PDB) and therefore a probable ecological event.

6. Conclusions

Although the original shell architecture is well preserved and organic growth lines are clearly visible without evidence of neomorphism, cathodoluminescence, scanning electron microscope and geochemical data (analyses of stable isotopes, minor, traces and REE) support the hypothesis of diagenetic modification, which becomes particularly evident in the inoceramid shells collected from the Sopelana and Zumaya sections and is observed to a lesser extent in those from Bidart. The diagenetic intensity shown by inoceramid, marl and marl-limestone oxygen isotopic values increases from east to west in the Basque Arc domain.

The lithology of the host-rock (marl or marly-limestone) in every section and the shell thickness do not seem to be strongly related to the grade of diagenetic alteration suffered by the inoceramid shell.

Inoceramid shells have a relatively heavy carbon isotopic composition which is close to that of the host sediment. For this reason, the hypothesis of a 'vital effect' upon the composition of shells cannot be maintained for the time being. Oxygen isotopic values are clearly lower in shells collected from Sopelana and Zumaya when compared with those from Bidart. The estimation of mean palaeotemperature based on the Sopelana and Zumaya shells is meaningless due to diagenetic processes, but the palaeotemperature value of 13ºC estimated from the non-luminescent middle shell layer (MSL) from the Bidart section seems to be compatible with values for palaeolatitudes of about 30ºN during mid-Maastrichtian time.

Cathodoluminescence is a useful tool for showing the paths of diagenetic fluids responsible for diagenetic modification. Whereas most shells collected from the Sopelana and Zumaya sites have their luminescence homogenized by diagenesis, with combined effects of intragranular cementation and recrystallization, those from Bidart still permit recognition of the paths for diagenetic fluids. At Bidart, diagenetic fluids followed the boundaries between prisms which seem to have been the most favourable

paths for diagenetic fluid advance from the outer shell layer (OSL) and the inner shell layer (ISL) to the middle shell layer (MSL).

Enrichment and depletion of minor, traces and REE values together with cationic zonations from the OSL or ISL to the middle parts of the shell are considered to be the result of cationic mobilization during diagenesis. Since it is the region least affected by diagenesis, the Bidart section turns out to be the most promising area as regards the study of palaeoenvironmental conditions that prevailed during mid-Maastrichtian time in the coastal region of the Bay of Biscay.

Acknowledgements

This study was funded by Research Projects UPV/EHU 130.310-EB059/93 and EB177/96 financed by the University of the Basque Country. Critical and constructive review of this manuscript by Drs. K.G. MacLeod (National Museum of Natural History, Smithsonian Institution, Washington, DC), J.D Marshall (Liverpool University) and K. Chinzei (Kyoto University) greatly improved the final manuscript. We would like to thank D.J. Fogarty (University of the Basque Country) for improving the English translation.

References

Barrera, E., 1994. Global environmental changes preceding the Cretaceous–Tertiary boundary: early–late Maastrichtian transition. Geology 22, 877–880.

Barrera, E., Huber, B.T., 1990. Evolution of Antarctic bottom waters during the Maestrichtian: Foraminifer oxygen and carbon isotope ratios, ODP Leg 113. Proc. ODP, Init. Rep. 113, 813–828.

Barrera, E., Tevesz, M.J.S., 1990. Oxygen and carbon isotopes: utility for environmental interpretation of Recent and fossil invertebrate skeletons. In: Carter, J.G. (Ed.), Skeletal Biomineralization: Pattern, Process and Evolutionary Trends. Van Nostrand, New York, pp. 557–566.

Barrera, E., Huber, B.T., Savin, S.M., Webb, P.N., 1987. Antartic marine temperatures: Late Campanian through Early Paleocene. Paleoceanography 2, 21–47.

Barrera, E., Tevesz, M.J.S., Carter, J.G., 1990. Variations in oxygen and carbon isotopic compositions and microstructure of the shell of *Adamussium colbecki* (Bivalvia). Palaios 5, 149–159.

Barron, E.J., Saltzman, E., Price, D.A., 1984. Occurrence of *Inoceramus* in the South Atlantic and oxygen isotopic paleotemperatures in Hole 530A. Init. Rep. DSDP 75, 893–904.

Boersma, A., 1984. Campanian through Paleocene paleotemperatures and carbon isotope sequence and the Cretaceous–Tertiary boundary in the Atlantic Ocean. In: Berggren, W.A., van Couvering, J.A. (Eds.), Catastrophes and Earth History. Princeton Univ. Press, Princeton, pp. 247–278.

Brand, U., 1986. Paleoenvironmental analysis of Middle Jurassic (Callovian) ammonoids from Poland: trace elements and stable isotopes. J. Paleontol. 60, 293–301.

Brand, U., 1987. Depositional analysis of the Breathitt Formation's marine horizons, Kentucky, U.S.A.: trace elements and stable isotopes. Chem. Geol. (Isot. Geosci. Sect.) 65, 117–136.

Brand, U., Morrison, J.O., 1987. Biogeochemistry of fossil marine invertebrates. Geosci. Can. 14, 85–107.

Burnett, J., Kennedy, W.J., Ward, P., 1992. Maastrichtian nannofossil biostratigraphy in the Biscay region (south-western France, northern Spain). Newsl. Stratigr. 26, 145–155.

Carson, G.A., 1987. Silicification fabrics from the Cenomanian and basal Turonian of Devon, England: Isotopic results. In: Marshall, J.D. (Ed.), Diagenesis of Sedimentary Sequences. Geol. Soc. London, Spec. Publ. 36, 87–102.

Clauser, S., 1987. Evolution de la composition isotopique de l'oxygène des carbonates durant le Campanien–Maastrichtien. Données préliminaires issues de la série de Bidart (Pyrénées–Atlantiques). C. R. Acad. Sci., Paris, Sér. II 304 (11), 579–584.

Clauser, S., 1994. Etudes stratigraphiques du Campanien et du Maastrichtien de l'Europe Occidentale: Cote Basque, Charentes (France), Limbourg (Pays-Bas). Doc. BRGM 235, 243 pp.

Craig, H., 1965. The measurement of oxygen isotope palaeotemperatures. In: Tongiorgi, E. (Ed.), Stable Isotopes in Oceanographic Studies and Palaeotemperatures. Consiglio Nazionale delle Richerche, Laboratorio di Geologia Nucleare, Pisa, pp. 161–182.

Crame, J.A., Luther, A., 1997. The last inoceramid bivalves in Antarctica. Cretaceous Res. 18, 179–195.

Crame, J.A., Lomas, S.A., Pirrie, D., Luther, A., 1996. Late Cretaceous extinction patterns in Antarctica. J. Geol. Soc. London 153, 503–506.

Delacotte, O., 1982. Etude magnétostratigraphique et géochimique de la limit Crétacé–Tertiaire de la Coupe de Bidart (Pyrénées Atlantique). 3ème cycle doctoral thesis, University of Paris, 162 pp. (unpublished, as cited in Mathey, 1988 and Clauser, 1987).

Delacotte, O., Renard, M., Laj, C., Perch-Nielsen, K., Premoli-Silva, I., Clauser, S., 1985. Magnétostratigraphie et biostratigraphie du passage Crétacé–Tertiaire de la Coupe de Bidart (Pyrénées Atlantiques). Geol. Fr. 3, 243–254.

D'Hondt, A.V., 1983. Campanian and Maastrichtian inoceramids: a review. Zitteliana 10, 689–701.

Dickson, J.A.D., 1965. A modified staining technique for carbonates in thin section. Nature 205, 587.

Ditchfield, P.W., Marshall, J.D., Pirrie, D., 1994. High latitude palaeotemperature variation: new data from the Tithonian

to Eocene of James Ross Island, Antarctica. Palaeogeogr., Palaeoclimatol., Palaeoecol. 107, 79–101.

Dodd, J.R., Stanton, R.J., 1981. Palaeocology, Concepts and Applications. Wiley, Chichester, 559 pp.

Elorza, J., García-Garmilla, F., 1996. Petrologic and geochemical evidence for diagenesis of inoceramid bivalve shells in the Plentzia Formation (Upper Cretaceous, Basque Cantabrian Region, Northern Spain). Cretaceous Res. 17, 479–503.

Elorza, J., García-Garmilla, F., Jagt, J.W.M., 1997. Diagenesis-related differences and elemental composition of late Campanian and early Maastrichtian inoceramids and belemnites from NE Belgium: palaeoenvironmental implications. Geol. Mijnbouw 75, 349–360.

Feuillée, P., Rat P., 1971. Structures et paléogéographies pyrénéo–cantabriques. In: Histoire Structurale du Golfe de Gascogne. Technip, Paris, p. V. 1-1 à V. 1-48.

Gorostidi, A., 1993. Nannofósiles calcáreos y eventos del Cretácico medio-superior de la Región Vasco–Cantábrica. Tésis Doctoral (inedita), Universidad del País Vasco, 304 pp.

Govindaraju, K., Mevelle, G., 1987. Fully automated dissolution and separation methods for inductively coupled plasma atomic emission spectrometry rock analysis. Application to determination of rare earth elements. J. Anal. Atom. Spectrom. 2, 615–621.

Henoc, J., Tong, M., 1978. Automatisation de la microsonde. J. Microsc. Spectrosc. Electron. 3, 247–254.

Hu, X., Wang, Y.L., Schmitt, R.A., 1988. Geochemistry of sediments on the Rio Grande Rise and the redox evolution of the South Atlantic Ocean. Geochim. Cosmochim. Acta 52, 201–207.

Huber, B.T., 1990. Maestrichtian planktonic foraminifera biostratigraphy of the Maud Rise (Weddell Sea, Antarctica); ODP leg 113 holes 689B and 690C. Proc. ODP, Sci. Results 113, 489–513.

Jenkyns, H.C., Gale, A.S., Corfield, R.M., 1994. Carbon- and oxygen-isotope stratigraphy of the English Chalk and Italian Scaglia and its palaeoclimatic significance. Geol. Mag. 131, 1–34.

Krantz, D.E., Williams, D.F., Jones, D.S., 1987. Ecological and paleoenvironmental information using stable isotope profiles from living and fossil molluscs. Palaeogeogr., Palaeoclimatol., Palaeoecol. 58, 249–266.

Lamolda, M.A., Orue-Etxebarria, X., Proto-Decima, F., 1983. The Cretaceous–Tertiary boundary in Sopelana (Biscay, Basque Country). Zitteliana 10, 663–670.

Lécuyer, C., Grandjean, P., O'Neil, H., Cappetta, H., Martineau, F., 1993. Thermal excursions in the ocean at the Cretaceous–Tertiary boundary (northern Morocco): $\delta^{18}O$ record of phosphatic fish debris. Palaeogeogr., Palaeoclimatol., Palaeoecol. 105, 235–243.

López, G., 1992. Paleontología y Bioestratigrafía de los inocerámicos (Bivalvia) del Cretácico Superior de la Cuenca Navarro–Cántabra y de la Plataforma Norcastellana, Parte I. Situación geológica de las series realizadas y estudio sistemático de los subgéneros *Inoceramus* Sowerby y *Cremnoceramus* Cox. Bol. Geol. Miner. 103, 210–252.

López, G., Martínez, R., Lamolda, M., 1992. Biogeographic relationships of the Coniacian and Santonian inoceramid bivalves of northern Spain. Palaeogeogr., Palaeoclimatol., Palaeoecol. 92, 249–261.

Lowenstam, H.M., 1964. Palaeotemperatures of the Permian and Cretaceous periods. In: Nairn, A.E.M. (Ed.), Problems in Palaeoclimatology. Wiley, Chichester, pp. 227–248.

MacLeod, K.G., 1994. Extinction of Inoceramid bivalves in Maastrichtian strata of the Bay of Biscay region of France and Spain. J. Paleontol. 68, 1048–1066.

MacLeod, K.G., Hoppe, K.A., 1992. Evidence that inoceramid bivalves were benthic and harbored chemosynthetic symbionts. Geology 20, 117–120.

MacLeod, K.G., Huber, B.T., Ward, P.D., 1996. The biostratigraphy and paleobiogeography of Maastrichtian inoceramids. In: Ryder, G., Fastovsky, D., Gartner, S. (Eds.), The Cretaceous–Tertiary Event and Other Catastrophes in Earth History. Geol. Soc. Am. Spec. Pap. 307, 361–373.

MacLeod, K.G., Orr, W.N., 1993. The taphonomy of Maastrichtian inoceramids in the Basque region of France and Spain and the pattern of their decline and disappearance. Paleobiology 19, 235–250.

MacLeod, K.G., Ward, P.D., 1990. Extinction pattern of *Inoceramus* (Bivalvia) based on shell fragment biostratigraphy. In: Sharpton, V.L., Ward, P.D. (Eds.), Global Catastrophes in Earth history. Geol. Soc. Am. Spec. Pap. 247, 509–518.

Margolis, S.V., Mount, J.F., Doehne, E., Showers, W., Ward, P., 1987. The Cretaceous/Tertiary boundary carbon and oxygen isotope stratigraphy, diagenesis, and paleoceanography at Zumaya, Spain. Paleoceanography 2, 361–377.

Marshall, J.D., 1992. Climatic and oceanographic isotopic signals from the carbonate rock record and their preservation. Geol. Mag. 129, 143–160.

Mary, C., Moreau, M.G., Orue-Etxebarria, X., Apellaniz, E., Courtillot, V., 1991. Biostratigraphy and magnetostratigraphy of the Cretaceous/Tertiary Sopelana section (Basque country). Earth Planet. Sci. Lett. 106, 133–150.

Mathey, B., 1982. El Cretácico Superior del Arco Vasco. In: El Cretácico de España. Universidad Complutense. Madrid, pp. 111–136.

Mathey, B., 1987. Les flyschs crétacé supérieur des Pyrénées basques. Mem. Géol. Univ. Dijon 12, 399 pp.

Mathey, B., 1988. Paleogeographical evolution of the Basco–Cantabrian Domain during the Upper Cretaceous. Rev. Esp. Paleontol. Número Extraordinario, pp. 142–147.

McArthur, J.M., Burnett, J., Hancock, J.M., 1992. Strontium isotopes at the K/T boundary: comment. Nature 355, 28.

McCrea, J.M., 1950. On the isotopic chemistry of carbonates and a paleotemperature scale. J. Chem. Phys. 18, 669–673.

Morrison, J.O., Brand, U., 1984. Secular and environmental variation of seawater: an example of brachiopod chemistry. Geol. Assoc. Can., Annu. Meet., Progr. Abstr. 9, 91.

Morrison, J.O., Brand, U., 1986. Geochemistry of Recent marine invertebrates. Geosci. Can. 13, 237–254.

Morrison, J.O., Brand, U., 1988. An evaluation of diagenesis and chemostratigraphy of Upper Cretaceous molluscs from the Canadian Interior Seaway. Chem. Geol. (Isot. Geosci. Sect.) 72, 235–248.

Mount, J.F., Ward, P., 1986. Origin of limestones/marl alternations in the upper Maastrichtian of Zumaya, Spain. J. Sediment. Petrol. 56, 228–236.

Mount, J.F., Margolis, S.V., Showers, W., Ward, P., Doehne, E., 1986. Carbon and oxygen isotope stratigraphy of the upper Maastrichtian, Zumaya, Spain: a record of oceanographic and biologic changes at the end of the Cretaceous Period. Palaios 1, 87–92.

Nelson, B.K., MacLeod, K.G., Ward, P.D., 1991. Rapid change in strontium isotopic composition of seawater prior to the Cretaceous/Tertiary boundary. Nature 351, 644–647.

Percival, S.F., Fischer, A.G., 1977. Changes in the calcareous nannoplankton in the Cretaceous–Tertiary biotic crisis at Zumaya, Spain. Evolutionary Theory 2, 1–35.

Pirrie, D., Marshall, J.D., 1990a. Diagenesis of *Inoceramus* and Late Cretaceous paleoenvironmental geochemistry: a case study from James Ross Island, Antarctica. Palaios 5, 336–345.

Pirrie, D., Marshall, J.D., 1990b. High-paleolatitude Late Cretaceous paleotemperatures: new data from James Ross Island, Antarctica. Geology 18, 31–34.

Ragland, P.C., Pilkey, O., Blackwelder, B.W., 1979. Diagenetic changes in the elemental composition of unrecrystallized mollusk shells. Chem. Geol. 25, 123–134.

Rat, P., 1959. Les pays crétacés basco–cantabriques. Publ. Université de Dijon, 18, 525 pp.

Rio, M., Roux, M., Renard, M., Schein, E., 1992. Chemical and isotopic features of present day bivalve shells from hydrothermal vents or cold seeps. Palaios 7, 351–360.

Saito, T., Van Donk, J., 1974. Oxygen and carbon isotope measurements of Late Cretaceous and Early Tertiary foraminifera. Micropaleontology 20, 152–177.

Saltzman, E.S., Barron, E.J., 1982. Deep circulation in the Late Cretaceous: oxygen isotope paleotemperatures from *Inoceramus* remains in D.S.D.P. cores. Palaeogeogr., Palaeoclimatol., Palaeoecol. 40, 167–181.

Schönfeld, J., Sirocko, F., Jørgensen, N.O., 1991. Oxygen isotope composition of Upper Cretaceous chalk at Lägerdorf (NW Germany): its original environmental signal and palaeotemperature interpretation. Cretaceous Res. 12, 27–46.

Shackleton, N., Hall, M.A., Boersma, A., 1984. Oxygen and carbon isotope data from Leg 74 foraminifera. Init. Rep. DSDP 74, 599–612.

Thomas, E., 1990. Late Cretaceous through Neogene deep-sea benthic foraminifers (Maud Rise, Weddell Sea, Antarctica): ODP leg 113 holes 689B and 690C. Proc. ODP, Sci. Results 113, 571–594.

Veizer, J., Fritz, P., Jones, B., 1986. Geochemistry of brachiopods: oxygen and carbon isotopic records of Paleozoic oceans. Geochim. Cosmochim. Acta 50, 1679–1696.

Voigt, S., 1995. Palaeobiogeography of early Late Cretaceous inoceramids in the context of a new global palaeogeography. Cretaceous Res. 16, 343–356.

von Hillebrandt, A., 1965. Foraminiferen-Stratigraphie im Altertiär von Zumaya (Provinz Guipuzcoa, NW Spanien) und ein Vergleich mit anderen Tethys-Gebieten. Bayer. Akad. Wiss. Math. Naturwiss. Kl., Abh., N.F. 123: 62 pp.

Wang, Y.L., Liu, Y.G., Schmitt, R.A., 1986. Rare earth element geochemistry of South Atlantic deep sea sediments: Ce anomaly change at −54 My. Geochim. Cosmochim. Acta 50, 1337–1355.

Ward, P.D., 1988. Maastrichtian ammonite and inoceramid ranges from Bay by Biscay Cretaceous–Tertiary boundary sections. Rev. Esp. Paleontol. Número Extraordinario, pp. 119–126.

Ward, P.D., Kennedy, W.J., 1993. Maastrichtian ammonite and inoceramid ranges from Biscay region. J. Paleontol. 34, 58 pp.

Ward, P.D., Wiedmann, J., Mount, J.F., 1986. Maastrichtian molluscan biostratigraphy and extinction patterns in a Cretaceous/Tertiary boundary section exposed at Zumaya, Spain. Geology 14, 899–903.

Ward, P.D., Kennedy, W.J., MacLeod, K.G., Mount, J., 1991. End-Cretaceous molluscan extinction patterns in Bay of Biscay K/T boundary sections: two different patterns. Geology 19, 1181–1184.

Ward, P.D., Nelson, B.K., MacLeod, K.G., 1992. Rapid change in strontium isotopic composition of seawater prior to the Cretaceous/Tertiary boundary: reply. Nature 358, 378.

Whittaker, S.G., Kyser, T.K., 1993. Variations in the neodymium and strontium isotopic composition and REE content of molluscan shells from the Cretaceous Western Interior Seaway. Geochim. Cosmochim. Acta 57, 4003–4014.

Whittaker, S.G., Kyser, T.K., Caldwell, W.G.E., 1987. Palaeoenvironmental geochemistry of the Claggett marine cyclotherm in south-central Saskatchewan. Can. J. Earth Sci. 24, 967–984.

Wiedmann, J., 1988a. The Basque coastal sections of the K/T boundary. A key to understanding 'mass extinction' in the fossil record. Rev. Esp. Paleontol. Número Extraordinario, pp. 127–140.

Wiedmann, J., 1988b. Ammonoid extinction and the 'Cretaceous–Tertiary Boundary Event' In: Wiedmann, J., Kullmann, J. (Eds.), Cephalopods — Present and Past. Schweizerbart, Stuttgart, pp. 117–140.

Wright, E.K., 1987. Stratification and paleocirculation of the Late Cretaceous Western Interior Seaway of North America. Geol. Soc. Am. Bull. 99, 480–490.